GEOPHYSICAL AND ASTROPHYSICAL FLUID DYNAMICS BEYOND THE TRADITIONAL APPROXIMATION

T. Gerkema,[1] J. T. F. Zimmerman,[1,2] L. R. M. Maas,[1,2] and H. van Haren[1]

[1] In studies on geophysical fluid dynamics, it is common practice to take the Coriolis force only partially into account by neglecting the components proportional to the cosine of latitude, the so-called traditional approximation (TA). This review deals with the consequences of abandoning the TA, based on evidence from numerical and theoretical studies and laboratory and field experiments. The phenomena most affected by the TA include mesoscale flows (Ekman spirals, deep convection, and equatorial jets) and internal waves. Abandoning the TA produces a tilt in convective plumes, produces a dependence on wind direction in Ekman spirals, and gives rise to a plethora of changes in internal wave behavior in weakly stratified layers, such as the existence of trapped short low-frequency waves, and a poleward extension of their habitat. In the astrophysical context of stars and gas giant planets, the TA affects the rate of tidal dissipation and also the patterns of thermal convection.

Citation: Gerkema, T., J. T. F. Zimmerman, L. R. M. Maas, and H. van Haren (2008), Geophysical and astrophysical fluid dynamics beyond the traditional approximation, *Rev. Geophys.*, *46*, RG2004, doi:10.1029/2006RG000220.

1. INTRODUCTION

[2] In a now famous memoir, *Coriolis* [1835] derived the equations of motion for rotating devices, in which he identified a deflecting force that he called "force centrifuge composée," now known as the Coriolis force. It acts on particles moving in the frame of reference of the rotating system, is proportional to their velocity, and produces a deflection in a direction perpendicular to velocity. The rotating "device" we are primarily concerned with in this paper is, of course, the Earth. The notion that the Earth's diurnal rotation produces a deflecting force had, in fact, been recognized before Coriolis, albeit initially in rudimentary form; in the 18th century, G. Hadley thus provided a qualitative explanation of the trade winds [*Burstyn*, 1966]. In a preamble to his dynamic theory of tides, *Laplace* [1798] derived the exact mathematical form of the deflecting force. Adopting a geographical coordinate system, he showed that there are four "Coriolis" terms, whose roles are indicated in Table 1 (an elementary derivation of each of these terms is provided in Appendix A).

[3] Of these four terms, two are proportional to the sine of latitude; the other two are proportional to the cosine. This distinction has a deeper, dynamical significance. The force associated with the sine terms is due to, and induces, only horizontal movements. In the cosine terms, on the other hand, the vertical direction is always involved: the associated force either is due to a vertical velocity or induces a vertical acceleration. (These effects are perhaps most readily appreciated by means of the following simple mechanical examples: (1) the eastward deflection of a stone dropped from a tower and (2) the upward force undergone by an eastward moving object, reducing its weight, the so-called Eötvös effect.) Exploiting this distinction, Laplace developed a chain of arguments which led him to conclude that while the sine terms are to be retained, the cosine terms can be neglected (see *Laplace* [1878, Livre I, sections 35 and 36]; for a valuable summary of this and other aspects of Laplace's tidal theory, see *Dubois* [1885]). In this, he has been followed almost universally in later studies on geophysical fluid dynamics (GFD), which inspired *Eckart* [1960] to coin the apt name "traditional approximation" (TA) to refer to the neglect of the cosine terms, i.e., the terms with $\tilde{f}$ in Table 1. The TA's widespread adoption notwithstanding, studies devoted to the role of $\tilde{f}$ have occasionally appeared since the late 1920s and more frequently so in recent years. As the interest in the topic has waxed and waned repeatedly, the literature is scattered, and much of it has slipped into oblivion. The principal goals of this review are to give a coherent overview of the existing literature, to pinpoint the kinds of motion in which $\tilde{f}$ is plausibly significant, and to outline the unresolved issues.

[1]Royal Netherlands Institute for Sea Research, Texel, Netherlands.
[2]Institute for Marine and Atmospheric Research, Utrecht University, Utrecht, Netherlands.

TABLE 1. Components of the Coriolis Acceleration[a]

Initial Velocity	Induced Coriolis Acceleration (Northern Hemisphere)
Eastward (u)	southward ($-fu$) and vertically upward ($\tilde{f}u$)
Northward (v)	eastward (fv)
Vertically upward (w)	westward ($-\tilde{f}w$)

[a]Here, $f = 2\Omega\sin\phi$ and $\tilde{f} = 2\Omega\cos\phi$, where Ω is the Earth's angular velocity (7.292×10^{-5} rad s^{-1}) and ϕ is latitude in the Northern Hemisphere. In the Southern Hemisphere, f is negative, so in the column on the right, "southward" is then replaced by "northward," and "eastward" is replaced by "westward."

[4] The justification for the TA centers around the observation that the depth of the oceans and atmosphere is very thin compared to the radius of the Earth; large-scale motions are therefore necessarily nearly horizontal. For Coriolis effects to be important, timescales need to be of the order of Ω^{-1} (the inverse Earth's angular velocity) or larger. Such low-frequency motions usually have large horizontal scales; the vertical motions must then be much weaker than the horizontal ones, rendering the Coriolis terms with $\tilde{f}$ insignificant compared to those with f and rendering the pressure field nearly hydrostatic. (Similarly, strong vertical stratification in density, which suppresses vertical motions, also diminishes the role of the $\tilde{f}$ terms.) This argument becomes, however, problematic near the equator (where $\tilde{f} \gg f$) and also in kinds of motion with a manifestly vertical character (such as deep convection) or for low-frequency motions with short horizontal scales (such as a class of internal waves discussed in section 6.1.2).

[5] The neglect of the $\tilde{f}$ terms conveniently aligns the remaining part of the rotation vector to gravity. This is illustrated in Figure 1, showing how at latitude ϕ the (full) rotation vector $\boldsymbol{\Omega}$ can be decomposed into a radial and meridional component; the former is proportional to f; the latter is proportional to $\tilde{f}$. Under the TA, only the radial component, aligned to gravity, is taken into account. Abandoning the TA breaks this symmetry: the rotation vector is then neither aligned to the vertical nor to the horizontal (except at the poles and equator), which implies, mathematically, that the set of partial differential equations that govern the motion cannot be solved by separation of horizontal and vertical variables. This, presumably, has often been taken as a practical (rather than a physically motivated) reason for making the TA.

[6] From Table 1 it is clear that the effect of f is isotropic in the horizontal geographical plane: it always produces an acceleration to the right with respect to velocity in the Northern Hemisphere (NH) and to the left in the Southern Hemisphere (SH), irrespective of the horizontal orientation of velocity. The component $\tilde{f}$, by contrast, introduces anisotropy in the horizontal plane: vertical velocities produce a zonal acceleration not a meridional one (third row of Table 1), and only zonal velocities produce a vertical acceleration (first row of Table 1). To summarize, we can identify three key elements of the nontraditional component $\tilde{f}$, which we will encounter repeatedly in this review: first, the crucial role of vertical movements (the Coriolis components with $\tilde{f}$ are due to a vertical current or induce a vertical acceleration); second, horizontal anisotropy, singling out zonal movements; and third, the tilt due to $\tilde{f}$ between the rotation vector and gravity, which is a source of nonseparability (i.e., mixed spatial derivatives in the governing partial differential equation).

[7] The TA may often be applicable in GFD but certainly not always; the present review is devoted to these exceptions. In sections 3–5 we discuss the role of $\tilde{f}$ in mesoscale motions, namely, Ekman flows, deep convection, and equatorial flows, a subject which has attracted much attention in recent years. Most of the literature questioning the TA has dealt with internal waves, which we address in section 6.1 (dynamics at a fixed latitude), where we also present observational work, and in section 6.2 (including latitudinal variation). The validity of the TA in the Laplace tidal equations has also been the subject of much debate (section 6.3). An excursion to the astrophysical context, finally, is made in section 7; here we focus on tidal oscillations and dissipation in giant planets and stars and on thermal convection. One of the conceptual problems of the TA is that it does not always stand by itself; for reasons of consistency, certain approximations need to be accompanied by the TA. Section 2 aims to discuss these connections. Readers who are primarily interested in the concrete manifestations of nontraditional effects may want to skip this section and consult it only when referred to in later sections.

2. MOMENTUM EQUATIONS: FROM THE ELLIPSOID TO THE f PLANE

[8] On the long geological timescale, the Earth has adjusted itself to the state of rotation; it has taken an oblate shape such that its surface forms, on the whole, a level of constant geopotential Φ (defined as the sum of gravitational and centrifugal potential). A fluid parcel at this level therefore experiences no tangential force so far as the geopotential is concerned. Overall, the surface closely
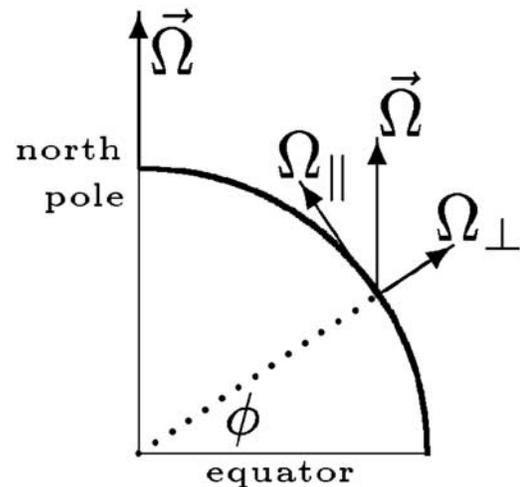
Figure 1. Decomposition of the rotation vector $\boldsymbol{\Omega}$ at latitude ϕ, giving rise to the components $f = 2\Omega_\perp$ and $\tilde{f} = 2\Omega_\|$. Under the TA, the terms associated with $\Omega_\|$ are neglected.

resembles an ellipsoid of revolution; hence it is natural to adopt oblate spherical coordinates [*Gates*, 2004]. However, anticipating later approximations (by which the ocean and atmosphere are treated as a spherical shell), we adopt spherical coordinates instead, so that the inviscid momentum equations become [e.g., *Veronis*, 1963a]:

$$\frac{D_s u_\lambda}{Dt} + \frac{u_\lambda w_r - u_\lambda v_\phi \tan\phi}{r} + 2\Omega w_r \cos\phi - 2\Omega v_\phi \sin\phi$$
$$= -\frac{1}{\rho r \cos\phi} \frac{\partial p}{\partial \lambda}, \tag{1}$$

$$\frac{D_s v_\phi}{Dt} + \frac{v_\phi w_r + u_\lambda^2 \tan\phi}{r} + 2\Omega u_\lambda \sin\phi = -\frac{1}{\rho r} \frac{\partial p}{\partial \phi} - \frac{1}{r} \frac{\partial \Phi}{\partial \phi}, \tag{2}$$

$$\frac{D_s w_r}{Dt} - \frac{u_\lambda^2 + v_\phi^2}{r} - 2\Omega u_\lambda \cos\phi = -\frac{1}{\rho} \frac{\partial p}{\partial r} - \frac{\partial \Phi}{\partial r}. \tag{3}$$

[9] Here λ is longitude, ϕ is latitude, r is the radius, and u_λ, v_ϕ, w_r are the associated velocity components; t is time, ρ denotes density, p is pressure, and Ω is the Earth's angular velocity (7.292×10^{-5} rad s^{-1}). The material derivative is defined as

$$\frac{D_s}{Dt} = \frac{\partial}{\partial t} + \frac{u_\lambda}{r\cos\phi}\frac{\partial}{\partial\lambda} + \frac{v_\phi}{r}\frac{\partial}{\partial\phi} + w_r\frac{\partial}{\partial r}.$$

On the left-hand side of (1)–(3), metric terms ( )/r are present, which are associated with advection. One also recognizes the four Coriolis terms of Table 1, here brought to the left-hand side. The terms $2\Omega w_r \cos\phi$ and $2\Omega u_\lambda \cos\phi$ are the ones neglected under the TA. For later reference, we note that the momentum equations (1)–(3) imply an exact conservation law for axial angular momentum:

$$\rho \frac{D_s}{Dt}[(u_\lambda + \Omega r\cos\phi)r\cos\phi] = -\frac{\partial p}{\partial\lambda}. \tag{4}$$

2.1. Thin-Layer Approximations

[10] The layers of the terrestrial atmosphere and oceans are very thin compared to the mean radius of the Earth (R); hence the inequality $|r - R|/R \ll 1$ is always satisfied, irrespective of the kind of motion under consideration. (Note that here we are comparing distances in the radial direction; any connotation with the "shallow water approximation," which refers to the aspect ratio, should be avoided.) This purely geometric fact, combined with the small eccentricity of the Earth's surface, suggests that we may treat the ocean and atmosphere as if they were a thin spherical shell. This entails several approximations. To begin with, for this approach to be consistent at all, spherical surfaces within the shell must act as levels of constant geopotential. A thorough analysis of this problem is given by *van der Toorn and Zimmerman* [2008]; the upshot is that in a lowest-order expansion involving three small parameters (eccentricity, relative shell thickness, and

relative rotation rate), the gradient $\partial\Phi/\partial\phi$ can indeed be neglected, while $\partial\Phi/\partial r$ reduces to a constant g.

[11] Another natural approximation, seemingly, is to replace r by R in the metric terms in (1)–(3), as is common practice in textbooks on GFD. However, *N. A. Phillips* [1966] showed that there is then no longer an exact conservation law for angular momentum. He proposed an alternative to avoid this problem; instead of the ad hoc replacement of r by R in (1)–(3), he introduced the thin-layer approximation in the metric tensor, which was then applied to the covariant form of the momentum equations. (An alternative derivation, using a variational principle, is given by *Müller* [1989] and in more detail by *White et al.* [2005].) This leads to the set

$$\frac{D'_s u_\lambda}{Dt} - \frac{u_\lambda v_\phi \tan\phi}{R} - 2\Omega v_\phi \sin\phi = -\frac{1}{\rho R\cos\phi}\frac{\partial p}{\partial\lambda}, \tag{5}$$

$$\frac{D'_s v_\phi}{Dt} + \frac{u_\lambda^2 \tan\phi}{R} + 2\Omega u_\lambda \sin\phi = -\frac{1}{\rho R}\frac{\partial p}{\partial\phi}, \tag{6}$$

$$\frac{D'_s w_r}{Dt} = -\frac{1}{\rho}\frac{\partial p}{\partial r} - g, \tag{7}$$

with

$$\frac{D'_s}{Dt} = \frac{\partial}{\partial t} + \frac{u_\lambda}{R\cos\phi}\frac{\partial}{\partial\lambda} + \frac{v_\phi}{R}\frac{\partial}{\partial\phi} + w_r\frac{\partial}{\partial r}.$$

[12] There is now an exact conservation law for axial angular momentum similar to the one in (4), with r replaced by R. But to achieve this, a number of terms have been "sacrificed," notably the Coriolis terms proportional to cos ϕ. In other words, this form of the thin-layer approximation implies the TA. (Still another way of introducing the thin-layer approximation was suggested by *Wangsness* [1970], but this leads to a conservation law for energy in which metric terms act as a source, which is "undesirable" [*Phillips*, 1970].) *Veronis* [1968] pointed out that the use of (5)–(7) may give a serious misrepresentation of the real physics, especially in equatorial regions, when the full rotation vector needs to be included. In other words, the TA, and hence the use of (5)–(7), cannot be justified on mere geometrical grounds (i.e., the shell being thin); the physical context must be considered.

[13] The somewhat intricate variety of thin-layer approximations can easily obscure the fact that we actually face a simple choice so far as the TA is concerned. The point is that the presence of nontraditional terms renders the problem nonseparable and hence, in spherical geometry, virtually impossible to solve analytically. For exact analytical treatment of nontraditional problems, one thus has to resort to more radical approximations that eliminate the spherical geometry still implied by the thin-layer approximation (see section 2.2). In numerical studies, on the other hand, there is no advantage in replacing r by R in the metric terms, and

one might as well use the original momentum equations (1)–(3) or their quasi-hydrostatic form, discussed in section 2.3, which too is dynamically consistent. The interpretation of numerical solutions requires, however, some care; even though it is tempting to think in terms of "normal modes" [e.g., *Thuburn et al.*, 2002a], this concept is not carried over straightforwardly from the traditional to the nontraditional setting because of the nonseparable nature of the solution in the latter case.

2.2. The β Plane and f Plane Approximations

[14] The β plane is a hybrid construction in the sense that one adopts a local Cartesian coordinate system (representing the Earth's surface as "flat"), while still preserving the variation of the Coriolis parameter(s) with latitude, which is due to the curvature of the Earth's surface. The β plane equations can be derived from (1)–(3) by appropriate scaling and then making an expansion in small parameters L/R and H/R, where L and H denote the characteristic horizontal and vertical scales, respectively, of the problem. The usual west-east, south-north, and vertical Cartesian coordinates are introduced via $x = (R\cos\phi_0)\lambda$, $y = R(\phi - \phi_0)$, and $z = r - R$, where ϕ_0 is the reference latitude around which the expansion is made. It is immediately clear from (1) and (2) that no proper transition to Cartesian coordinates is possible near the poles, since the metric terms proportional to $\tan\phi$ become infinite there (this is due to the nongeodesic character of spherical coordinates [see *Verkley*, 1990]). Sufficiently far away from the poles, however, one can make an expansion as presented by *LeBlond and Mysak* [1978]. This results in a set from which metric terms are absent and which is expressed in terms of the coordinates x, y, and z and their associated velocities u, v, and w:

$$\frac{Du}{Dt} + \tilde{f}w - fv = -\frac{1}{\rho}\frac{\partial p}{\partial x} \qquad (8)$$

$$\frac{Dv}{Dt} + fu = -\frac{1}{\rho}\frac{\partial p}{\partial y} \qquad (9)$$

$$\frac{Dw}{Dt} - \tilde{f}u = -\frac{1}{\rho}\frac{\partial p}{\partial z} - g, \qquad (10)$$

with $D/Dt = \partial/\partial t + \mathbf{u} \cdot \nabla$. The Coriolis parameters $\tilde{f}$ and f stem from a Taylor expansion of $2\Omega\cos(\phi_0 + y/R)$ and $2\Omega\sin(\phi_0 + y/R)$, respectively:

$$\tilde{f} = 2\Omega\cos\phi_0, \ \ f = 2\Omega\sin\phi_0 + \beta y, \ \ \text{where } \beta = 2\Omega\cos\phi_0/R. \qquad (11)$$

Here the linear term in y is included in the expansion of the "traditional" f term, thus allowing for effects of its latitudinal variation. In the "nontraditional" $\tilde{f}$ term, however, only the first (i.e., constant) term of the expansion is retained. The reason for ignoring the meridional dependence here lies not in the derivation as such but

rather in the a posteriori consideration of conservation laws. It was shown by *Grimshaw* [1975b] that the β plane equations (8–10) do imply angular momentum and vorticity conservation laws if $\tilde{f}$ is taken to be constant, while they do not if $\tilde{f}$ varies with y. There are perhaps not many problems in which the β effect and nontraditional effects are both important, but they are arguably so for near-inertial internal waves. As discussed below, there are in that case also dynamical reasons why the latitudinal variation of f matters, whereas that of $\tilde{f}$ does not. This lends further validity to the approximation (11) proposed by *Grimshaw* [1975b]. On the f plane, finally, the β term is neglected so that f and $\tilde{f}$ are now both treated as constants; this renders the momentum equations (8)–(10) dynamically fully consistent.

2.3. Hydrostatic and Quasi-hydrostatic Approximations

[15] The hydrostatic approximation means that the pressure at any point depends only on the weight of the fluid column above it; this amounts to replacing (10) by

$$\frac{\partial p}{\partial z} = -\rho g, \qquad (12)$$

the hydrostatic balance. (Similarly, in spherical coordinates, one replaces (3) by $\partial p/\partial r = -\rho\partial\Phi/\partial r$.) One is now forced to neglect also the term $\tilde{f}w$ in (8), lest the Coriolis force does work (as can be seen by multiplying (8), (9), and (12) by u, v, and w, respectively, and summing the resulting equations in order to make an energy equation). In other words, consistency requires that the hydrostatic approximation be accompanied by the TA.

[16] The principal advantage of making the hydrostatic approximation in theoretical and especially in numerical studies lies not so much in the assumption of the hydrostatic balance per se, as in the removal of the time derivative from the vertical momentum equation. This has led several authors [*White and Bromley*, 1995; *Marshall et al.*, 1997; *White et al.*, 2005] to propose an alternative, the quasi-hydrostatic approximation, which means that one replaces (10) by an equation from which only the material derivative is removed:

$$-\tilde{f}u = -\frac{1}{\rho}\frac{\partial p}{\partial z} - g, \qquad (13)$$

the quasi-hydrostatic balance. (Similarly, in (3) one removes $D_s w_r/Dt$ while retaining the metric and Coriolis terms.) Clearly, the nontraditional terms can coexist with the quasi-hydrostatic approximation. *White and Bromley* [1995] and *White et al.* [2005] showed that the quasi-hydrostatic momentum equations are dynamically consistent and that they correctly imply conservation laws for energy, angular momentum, and potential vorticity.

[17] In summary, the following versions of the momentum equations, with nontraditional terms included, can be considered dynamically consistent: first, the full version in spherical coordinates (1)–(3); second, its quasi-hydrostatic
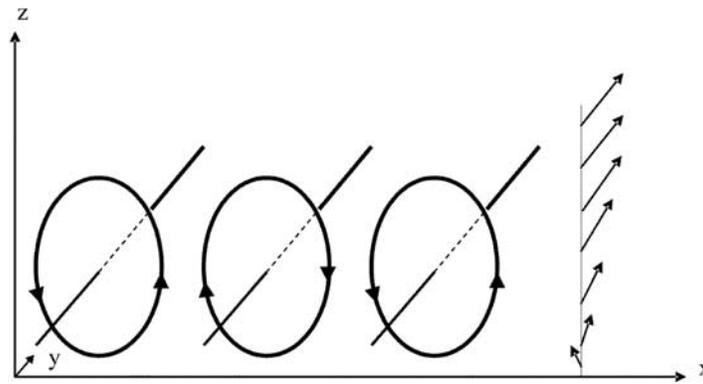
Figure 2. Sketch of vortex rolls due to the instability of the Ekman layer beneath the geostropic wind. On the right, the arrows indicate the wind, being geostrophic at high positions (directed along y) and turning anticlockwise in the downward direction in the Ekman layer; near the bottom, the angle is $45°$ to the left of the geostrophic wind. Within the Ekman layer, instabilities in the form of vortex rolls appear, depicted on the left. Their main axis is typically nearly aligned to the geostrophic wind.

version; third, the approximated momentum equations on the f plane (8)−(10); fourth, the corresponding quasi-hydrostatic version with (10) replaced by (13). In the β plane version, consistency requires that $\tilde{f}$ be taken constant.

3. EKMAN FLOWS

[18] In the classical paper by *Ekman* [1905], the friction layers at the bottom of ocean or atmosphere and at the top of the ocean are typical "traditional" flows. They are purely horizontal and suppose a dynamic balance between the traditional components of the Coriolis acceleration and the divergence of vertical momentum transport by a constant viscosity (which may be thought of as an eddy viscosity representing small-scale turbulence). Since the nontraditional components do not enter the problem, the classical Ekman solution is characterized by horizontal isotropy: a change in the forcing direction produces a corresponding change in the orientation of the response, but otherwise, the response remains the same; its structure as such does not depend on the forcing direction. ("Forcing" here means either the applied wind stress at the top of the ocean, the so-called "oceanic" case, or the external geostrophic current over a rigid bottom, the "atmospheric" case.) Besides this absence of the influence of forcing direction, the principal outcome of the classical Ekman problem is the direction of the surface current, being $45°$ to the right (left) of the applied stress in the NH (SH). As a matter of fact, observed angles usually deviate significantly from this value; Ekman himself discussed observations by Nansen, who had observed deflection angles substantially less than $45°$, i.e., between $20°$ and $40°$. Interestingly, this is counter to the result of an important modification that Ekman introduced at the end of his 1905 paper. There he discusses the case of an eddy viscosity that depends on the vertical shear of the current. This makes the eddy viscosity a function of depth, which renders the problem nonlinear though still integrable. It results in two properties that deviate from the constant

viscosity solution: the layer is not exponentially decaying but becomes of finite depth, and the deflection angle becomes slightly larger than $45°$. In spite of the latter result, by relating vertical shear and eddy viscosity Ekman was on the right track to a more sophisticated boundary layer theory that recognizes the instability of the shear flow, its generation of coherent roll vortices, and, finally, the creation of large-scale turbulence, i.e., eddies with a size of the Ekman layer depth. These motions, which are disturbances on the mean Ekman shear flow, react back to the mean flow itself by creating enhanced vertical momentum transport. As these motions have substantial vertical velocities, they are subject to the full Coriolis acceleration and hence must bear signs of the anisotropy inherent to the full Coriolis force. This, in turn, must translate into effective eddy coefficients that depend not only on depth but also on the direction of the forcing, and this may have its bearing on the deflection angle. This is the route on which the rest of this section focuses.

3.1. Ekman Layer Instability: Vortex Rolls

[19] The classical Ekman flow may become unstable, giving rise to the formation of vortex rolls. These vortices take the form of a rotational motion around horizontal axes as shown in Figure 2, where the axes are (horizontally) tilted with respect to the geostrophic current at an angle of typically less than $20°$ (to the left or right). The dominant underlying mechanism of the instability can be convection (if the static stratification is unstable) or shear [*Etling*, 1971]; the two cannot always be clearly distinguished.

[20] As mentioned in section 3, the geostrophic and mean Ekman currents are purely horizontal; hence the effect of $\tilde{f}$ is limited to a modification of the hydrostatic balance, see (13). *Ekman* [1932] argued that this effect is extremely small. For the vortex rolls, arising from the instability of the Ekman layer, the situation is very different since they do involve vertical motions. This has led *Wippermann* [1969], and later authors, to split the problem into two parts: the basic flow, which is treated under the TA, and the instability problem, in which $\tilde{f}$ is taken into account. In linear instability
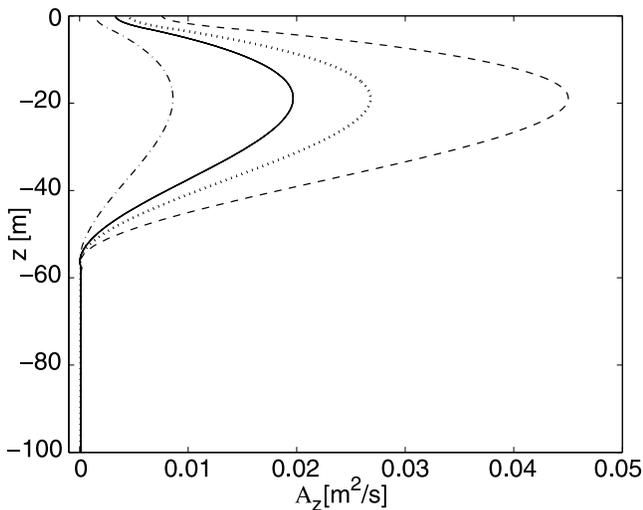
Figure 3. Effective eddy viscosity profiles for different wind directions. The solid line represents the profile under TA, in which case there is no dependence on wind direction. The other three lines include the effect of $\tilde{f}$: the largest values occur for winds to the SW (dashed line), the smallest occur for winds to the NE (dash-dotted line), and the intermediate case (dotted line) is for winds to the NW or SE. From *McWilliams and Huckle* [2006].

theory, the perturbation (i.e., vortex rolls) is assumed to be weak; *Wippermann* [1969] derived the equations for the vertical structure functions of the perturbation, assuming plane wave propagation in the horizontal direction at a certain angle ϵ with the basic geostrophic flow.

[21] *Etling* [1971] analyzed numerically some parameter regimes for unstable, neutral, and stable stratification. The neutral case was later examined more systematically by *Leibovich and Lele* [1985]. In the context of this review, the principal outcome of both studies is that the horizontal component $\tilde{f}$ plays an important role in that it introduces a dependence on the direction of the geostrophic flow in the horizontal geographical plane. Specifically, the threshold for instability is reduced most strongly if the axes of the vortex rolls are oriented west-east, with a near easterly geostrophic flow (i.e., directed to the west); beyond this threshold, moreover, growth rates are significantly enhanced. In a sequel to this work, a nonlinear instability analysis was carried out by *Haeusser and Leibovich* [1997, 2003]. They derived a coupled pair of differential equations for the amplitude of the rolls (anisotropic two-dimensional complex Ginzburg-Landau equation) and for the mean drift (Poisson equation). The resulting patterns reveal "defects," the intensity of which is much higher for easterly than for northwesterly winds, which presumably can be interpreted as enhanced small-scale turbulence in the former case. We note that all of the above mentioned studies assume constant eddy viscosity.

3.2. Vertical Turbulent Transfer

[22] In a direct numerical simulation (DNS), *Coleman et al.* [1990] studied the effect of $\tilde{f}$ on an atmospheric Ekman layer by doing model runs for four different wind directions.

The most extreme cases turn out to be an easterly versus westerly wind; at latitude 45°N, quantities like the frictional velocity and the angle of the stress at the bottom (with respect to the geostropic current) differ by as much as 6% and 30% between these extremes. The case with an easterly wind can be characterized as the most turbulent. *Coleman et al.* [1990] explain the difference by noting that $\tilde{f}$ brings about a redistribution of turbulent kinetic energy (TKE) between its horizontal and vertical components. This argument is developed in more detail by *Zikanov et al.* [2003], who carried out a large-eddy simulation (LES) for various parameter regimes of the wind-induced turbulent Ekman layer in the upper ocean. (The paper by *Zikanov et al.* [2003] states, however, some of the signs of the nontraditional terms incorrectly. For a correct reading, the angle γ defining the wind direction should be replaced by $-\gamma$; as a consequence, "west" and "east" should be interchanged throughout their text.) They point out that $\tilde{f}$ has a dual role: it affects the vertical turbulent momentum transfer, and (as noted already) it redistributes TKE between its horizontal and vertical components. Unlike f, which creates only an isotropic coupling between horizontal fluctuations [see *Tritton*, 1978], $\tilde{f}$ provides a coupling between horizontal and vertical fluctuations and introduces an anisotropy in the horizontal plane. The vertical turbulent momentum transfer, changed by $\tilde{f}$, in turn, affects the mean flow and the turbulence production by the mean shear.

[23] *Zikanov et al.* [2003], moreover, present an intuitively appealing method to incorporate these effects in a simple way. On the basis of their model results, they construct a vertically dependent effective eddy viscosity $A_z(z)$. This A_z turns out to depend strongly on the wind direction (all other parameters being the same), a manifestation of the change in turbulent momentum transfer due to $\tilde{f}$. For example, at latitude 15°N the maximum of A_z found for northeasterly winds exceeds the maximum for southwesterly winds by as much as a factor of 5. If one now takes these profiles as a starting point, the Ekman flow can be reconstructed; *Zikanov et al.* [2003] show that the flow thus obtained shares the principal characteristics with the mean flow produced by LES. The effect of $\tilde{f}$ is thus transferred, via A_z, to the Ekman flow. This idea was later extended by *McWilliams and Huckle* [2006], who incorporated $\tilde{f}$ and the resulting dependence on wind direction in a representation of the effective eddy viscosity profiles in the ocean Ekman layer (see Figure 3); $\tilde{f}$ was also found to alter significantly the response to time-variable wind, e.g., the direction of the surface current.

[24] A related issue is the possible influence of $\tilde{f}$ on the mixed layer depth. *Garwood et al.* [1985a] argued that $\tilde{f}$, combined with easterly winds, would deepen the mixed layer. *Garwood et al.* [1985b] applied this idea to the equatorial Pacific to explain the observed fact that the depth of the mixed layer increases substantially toward the west. However, *Galperin et al.* [1989], using a numerical model, did not find a significant influence of $\tilde{f}$ on mixed layer depth. It seems indeed more plausible that the observed deepening is simply due to horizontal convergence of mass
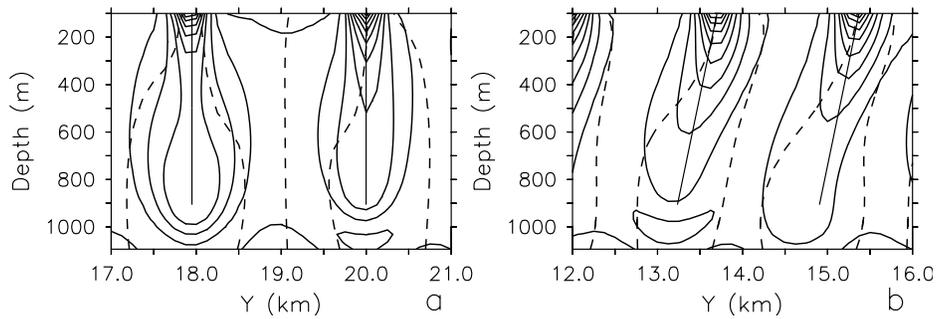
Figure 4. Convection simulated with a nonhydrostatic Boussinesq model, using parameter values appropriate for the Labrador Sea in (a) under the TA and (b) with $\tilde{f}$ included. Y is the meridional coordinate (poleward to the right). Solid lines follow isopycnals (contour interval 5×10^{-6} m s^{-2}); dashed lines indicate surfaces of constant "zonal absolute momentum," defined as $u - fy + \tilde{f}z$ (contour interval 0.1 m s^{-1}). The straight solid lines represent a prediction of plume orientation from an analytical model. From *Straneo et al.* [2002].

in the warm upper layer, driven by the westward mean wind stress [*Lukas and Lindstrom*, 1991].

[25] We note that the studies by *Coleman et al.* [1990], *Zikanov et al.* [2003], and *McWilliams and Huckle* [2006] assume a neutrally stratified Ekman layer. Stratification is known to affect the characteristics of the Ekman spiral (see, e.g., *Price and Sundermeyer* [1999] for an overview). One would expect that stable stratification diminishes the role of $\tilde{f}$ and hence the dependence on wind direction, but this has not yet been looked into.

4. DEEP CONVECTION

[26] In the Labrador, Greenland, and Weddell seas, deep water is intermittently formed by deep convection in plumes with a horizontal extent of the order of 1 km, in which vertical velocities can be as high as 10 cm s^{-1} [*Marshall and Schott*, 1999]. Apart from these high-latitude regions, convection also occurs in the Mediterranean (e.g., Gulf of Lions).

[27] Deep convection, with its strong vertical motions, seems a plausible candidate for a clear manifestation of the nontraditional component $\tilde{f}$. Several studies have been devoted to this aspect, most of them numerical. *Garwood* [1991] found a dependence on wind direction in numerical experiments on forced convection; for easterly winds a transfer was found to take place from horizontal to vertical TKE, while the reverse was the case for westerly winds. As a consequence, the mixed layer depth was larger (by about a factor of 2) in the former case. This result is in line with the discussion in section 3.2 on TKE in Ekman flows. *Denbo and Skyllingstad* [1996] looked into the structure of the plume and found that $\tilde{f}$ creates horizontal asymmetries, a manifestation of the horizontal anisotropy introduced by $\tilde{f}$.

[28] *Marshall and Schott* [1999] point out that lateral inhomogeneities such as shear currents or fronts, or indeed $\tilde{f}$, cause the convection to occur along slanted rather than strictly vertical paths. In the absence of other lateral

inhomogeneities, $\tilde{f}$ alone creates a tilt along the rotation axis; this follows from (8), with derivatives taken to be zero:

$$-fy + \tilde{f}z = \text{const.}$$

Looking downward, the tilt is toward the equator in both hemispheres. This effect is clearly visible in results from nonhydrostatic numerical models [*Straneo et al.*, 2002; *Wirth and Barnier*, 2006, 2008]; see Figure 4. This finding that mixing takes place along the axis of rotation rather than in the direction of gravity has important observational implications. Measurements are, of course, taken along vertical profiles, which means that one crosses tilted plumes rather than penetrating them. Interestingly, observations in the Labrador Sea by *Pickart et al.* [2002] indeed reveal convective sublayers; they put forward slantwise convection as a possible explanation. This would, however, not be necessarily due to $\tilde{f}$ alone since, as noted, other lateral inhomogeneities can also cause a tilt.

[29] In a series of ingenious "nontraditional" laboratory experiments on convection, *Sheremet* [2004] demonstrated a tilting of plumes caused solely by $\tilde{f}$. (The experiment was later carried out with sinking balls [see *Riemenschneider and Sheremet*, 2006].) In this setting (see Figure 5), a platform rotates at a rate Ω on a vertical axis; a tank is placed at a certain distance (R) from the axis. The fluid in the tank experiences an effective gravity formed by the vectorial sum of vertical gravity g and the horizontal centrifugal acceleration $\Omega^2 R$ and is thus directed at an angle α with the vertical, with $\tan\alpha = \Omega^2 R/g$. The surface of the fluid aligns itself to the level of constant "geopotential," the well-known parabolic shape; within the small tank, its curvature can, however, be neglected. The tank is placed such that its bottom is parallel to the free surface.

[30] The angle α between the rotation axis and effective gravity introduces nontraditional terms proportional to $2\Omega\sin\alpha$, formally similar to those in the geophysical context if we set $\alpha = 90° - \phi$, where ϕ is latitude. The tilt of the plumes is, indeed, very similar to those found in the numerical experiments by *Straneo et al.* [2002] and *Wirth*
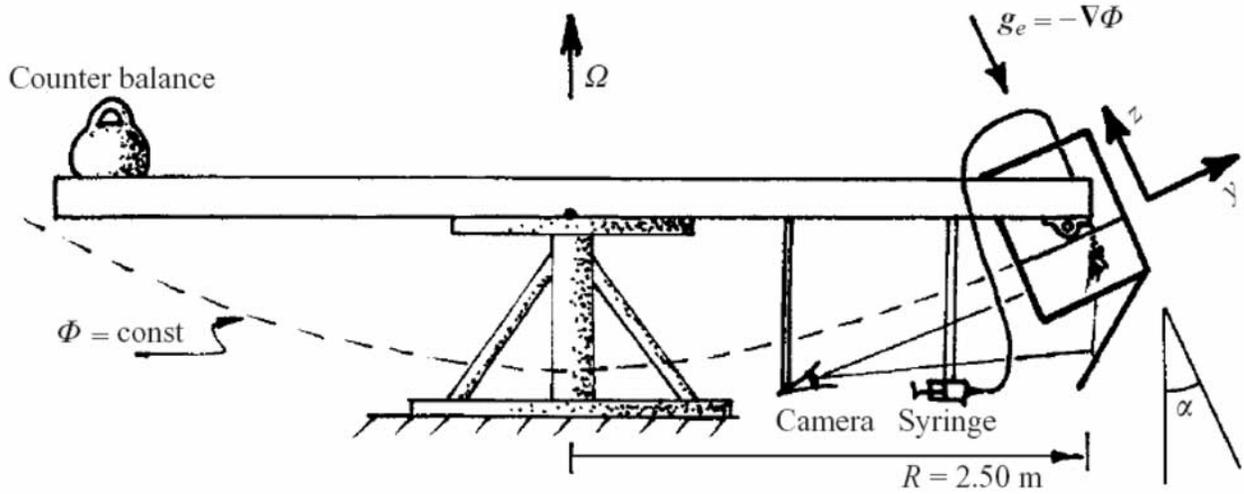
Figure 5. Sketch of the rotating platform used for "nontraditional" convection experiments. From *Sheremet* [2004]. Reprinted by permission from Cambridge University Press.

and Barnier [2006]; Figure 6 shows an initial and more developed stage of convection, in which the view is adjusted to the geographical setting. Although initially near vertical (Figure 6a), the plume is nearly aligned to the rotation axis at later stages and directed toward the "equator" (Figure 6b). Moreover, *Sheremet* [2004] found a small tilt toward the "east" (not shown here), as can be expected for a downward plume (see Table 1).

[31] Convection is not the only phenomenon in which $\tilde{f}$ creates a tilt. Theory predicts that so-called "meddies" (mesoscale anticyclonic lenses in the deep ocean) undergo a small tilt in their rotation axis if the TA is abandoned. These meddies typically have horizontal scales of 100 km and vertical scales of 100 m. *Lavrovskii et al.* [2000] and *Semenova and Slezkin* [2003] discuss the orientation of triaxial ellipsoidal lenses of homogeneous density submerged in a linearly stratified fluid of constant buoyancy frequency N. Incorporating the full Coriolis acceleration, these lenses appear to have a tilt in the sense that the line connecting the centers of horizontal circulation in the ellipsoid is inclined with respect to the vertical (see Figure 7). The slope of this tilt is given by $k = \tilde{f}/(f + \omega)$, where 2ω is the vertical component of the relative vorticity. The tilt of the line is poleward in the upward direction and is for characteristic midlatitude values of the parameters of the order of $60°-80°$. Similarly, there is an inclination in the same direction of the major axis of the ellipsoid with respect to the horizontal at an angle α, which can be approximated as $\alpha = |\omega|\tilde{f}/N^2$, which gives a rather small angle of the order of $0.01°$. Clearly, in this theory, both inclinations would vanish under the TA.
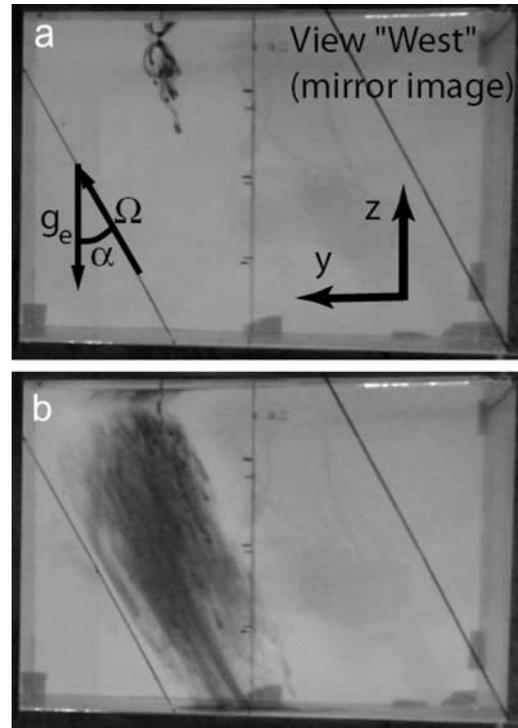
5. NEAR-EQUATORIAL FLOWS

5.1. Thermal Wind Balance

[32] At midlatitudes, the assumption of geostrophy leads to the well-known expressions for the "thermal wind balance," based on the TA, which have been widely adopted in meteorology and oceanography to deduce velocity fields from density measurements:

$$f\frac{\partial u}{\partial z} = \frac{g}{\rho_*}\frac{\partial \rho}{\partial y}; \quad f\frac{\partial v}{\partial z} = -\frac{g}{\rho_*}\frac{\partial \rho}{\partial x}. \tag{14}$$

Figure 6. Laboratory experiments on "nontraditional" convection: (a) the plume at an early stage and (b) the fully developed, tilted plume. In geophysical terms, the horizontal refers to the meridional coordinate (poleward to the left). From *Sheremet* [2004]. Reprinted by permission from Cambridge University Press.
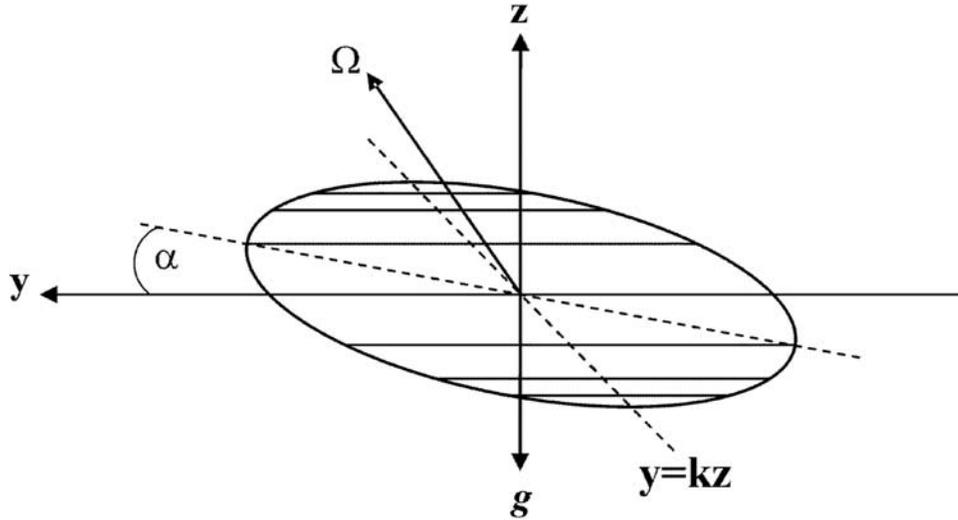
Figure 7. Meridional cross section of a "meddy" with a tilt due to $\tilde{f}$, following *Semenova and Slezkin* [2003]. The line with steepness k connects the centers of circulation at each depth, and α represents the tilt of the major axis. North is to the left (Northern Hemisphere).

(Here ρ_* is a constant reference value of density.) Thus, meridional density gradients are linked to vertical gradients of the zonal velocity and vice versa. These expressions obviously fail close to the equator, where $f \rightarrow 0$.

[33] A generalized formulation of the thermal wind balance, valid at any latitude including the equator, was derived by *Colin de Verdière and Schopp* [1994]. In their simplest form, the equations governing this balance can be obtained from the momentum equations in spherical coordinates (1)–(3), if one neglects the advective terms by assuming $D_s/Dt = 0$ and also the associated metric terms. This gives a nontraditional geostrophic balance in the zonal and meridional directions and the quasi-hydrostatic balance in the vertical. The pressure gradients can then be eliminated, resulting in

$$\frac{\tilde{f}}{r}\frac{\partial u}{\partial \phi} + f\frac{\partial u}{\partial r} = \frac{g}{\rho_*}\frac{\partial \rho}{r\,\partial \phi}, \tag{15}$$

$$\frac{\tilde{f}}{r}\frac{\partial v}{\partial \phi} + f\frac{\partial v}{\partial r} + \frac{\tilde{f}w}{r} = -\frac{g}{\rho_* r \cos\phi}\frac{\partial \rho}{\partial \lambda}, \tag{16}$$

$$\frac{\tilde{f}}{r}\frac{\partial w}{\partial \phi} + f\frac{\partial w}{\partial r} - \frac{\tilde{f}v}{r} = 0, \tag{17}$$

where $f = 2\Omega\sin\phi$ and $\tilde{f} = 2\Omega\cos\phi$ retain their full dependence on latitude (as opposed to their usage on the f and β planes). In deriving (16) and (17), use was made of the continuity equation in spherical coordinates. (We note that the signs of the last terms on the left-hand sides of (16) and (17) are stated incorrectly in the introduction of the paper by *Colin de Verdière and Schopp* [1994], but they are correct in their equation (11).) Equations (15) and (16) are the nontraditional generalizations of (14), while (17) is a generalization of an expression underlying the Sverdrup

balance. Zonal and meridional density gradients are now no longer related to vertical gradients of velocity but to the gradient of velocity projected onto the rotation vector $2\Omega = (0, \tilde{f}, f)$, as is clear from the fact that the Coriolis terms in (15) and (16) can be written as $(2\Omega \cdot \nabla)u$ and $(2\Omega \cdot \nabla)v$, respectively (∇ in spherical coordinates). Strictly, at the equator, one thus finds that horizontal density gradients are related to meridional gradients in velocity.

[34] In the derivation as we sketched it, nonlinear terms are wholly neglected, implying that we assume weak flows (i.e., small Rossby number: $U/2\Omega L$, where U and L are velocity and length scales, respectively). A careful scaling analysis and expansion, described by *Colin de Verdière and Schopp* [1994], shows, however, that (15) remains valid even for finite amplitude flows as long as the flow is meridionally confined; this generality is, however, not shared by (16).

[35] *Veronis* [1963b] derived a condition for neglecting the nontraditional terms: $\delta \ll \tan\phi$ (with aspect ratio $\delta = H/L$), which for small ϕ (in radians) reduces to $\delta \ll \phi \approx L/R$, or $L \gg (HR)^{1/2}$; the same criterion was obtained by *Colin de Verdière and Schopp* [1994]. This means that the nontraditional terms should generally be included for flows occurring within 200 km of the equator or two degrees in latitude. Indeed, as *Colin de Verdière and Schopp* [1994, p. 244] note, "The fact that considerable energy is found at low latitudes in the form of zonal jets on these lateral scales indicates that the traditional approximation should be seriously questioned."

[36] The generalized expressions (15) and (16) still await observational verification. *Joyce et al.* [1988] compared observational results (from profiling current meters and salinity/temperature measurements) with nontraditional equatorial β plane equations, which imply a set similar to (15)–(17); in particular, a quasi-hydrostatic balance was assumed as in (13). The deviation from a purely hydrostatic balance was found to be significant, although it improved the comparison only partially.
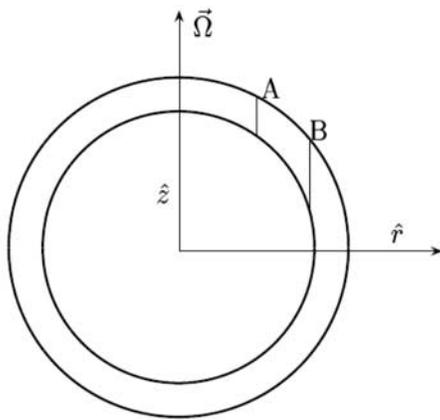
Figure 8. Taylor columns A and B between two concentric spherical surfaces, oriented parallel to the rotation axis $\vec{\Omega}$. The height of the column varies with latitude. The cylindrical coordinates $\hat{z}$ and $\hat{r}$ are also indicated (the third coordinate, azimuthal angle ψ, is not shown).

5.2. An Alternative View: Cylindrical Coordinates and Taylor Columns

[37] The common usage in GFD of spherical coordinates (section 2.1) or local Cartesian approximations thereof (section 2.2) is naturally motivated by the (near) spherical geometry of the Earth and the fact that the effective gravity acts in the vertical direction. The Earth's rotation, on the other hand, fits in awkwardly unless the TA is made, in which case the rotation vector becomes aligned to gravity (Figure 1). It is in this respect illuminating to change perspective by giving primacy to the Earth's rotation; this is done if one uses cylindrical coordinates: ψ (azimuthal angle), $\hat{r}$ (radial distance from the rotation axis), and $\hat{z}$ (distance along the rotation axis) and associated velocity components $\hat{u}$, $\hat{v}$, and $\hat{w}$. We briefly present some of the ideas put forward along these lines by *Schopp and Colin de Verdière* [1997] and *Colin de Verdière* [2002].

[38] In cylindrical coordinates, the geostrophic and hydrostatic balances read

$$-2\Omega\hat{v} = -\frac{1}{\rho}\frac{\partial p}{\hat{r}\partial\psi}, \tag{18}$$

$$2\Omega\hat{u} = -\frac{1}{\rho}\frac{\partial p}{\partial\hat{r}} - g\cos\phi, \tag{19}$$

$$\frac{\partial p}{\partial\hat{z}} = -\rho g\sin\phi, \tag{20}$$

where $\phi = \arctan(\hat{z}/\hat{r})$ denotes, as before, latitude. Note that the Coriolis force is present here in complete and exact form yet involves no more than two terms with constant coefficient 2Ω! This invites the question as to what has happened to the "β effect." The answer is sketched in Figure 8. Considering a spherical shell, one finds that the height of the water column, measured along the rotation axis, varies with latitude; specifically, it stretches as one approaches the equator. This stretching is none but the β effect in disguised form.

[39] Combining (18)–(20) into vorticity equations, one finds that for a homogeneous fluid (ρ constant), each of the velocity components must be uniform along the rotation axis (i.e., $\partial/\partial\hat{z} = 0$), the Taylor-Proudman theorem. Thus, motions take the form of Taylor columns whose axes are directed parallel to the rotation axis. They can move freely zonally but not meridionally since this would involve column stretching. *Schopp and Colin de Verdière* [1997] point out, however, that the column can move to other latitudes if one includes appropriate sources and sinks to compensate the column stretching. In particular, fluid parcels can cross the equator if the forcing is not symmetric.

[40] These elegant principles are, of course, not directly applicable to the ocean or atmosphere since both are stratified. They may, however, be quite relevant in the astrophysical context (see section 7.2).

5.3. Deep Equatorial Jets

[41] In the immediate vicinity of the equator, in a band of approximately 2°S to 2°N, deep zonal jets often appear in the ocean in a vertically stacked, or "pancake," form [*Luyten and Swallow*, 1976; *Firing*, 1987]; see Figure 9. Salinity anomalies equally reveal stacked structures [*Richards and Banks*, 2002]. A mechanism for their formation,
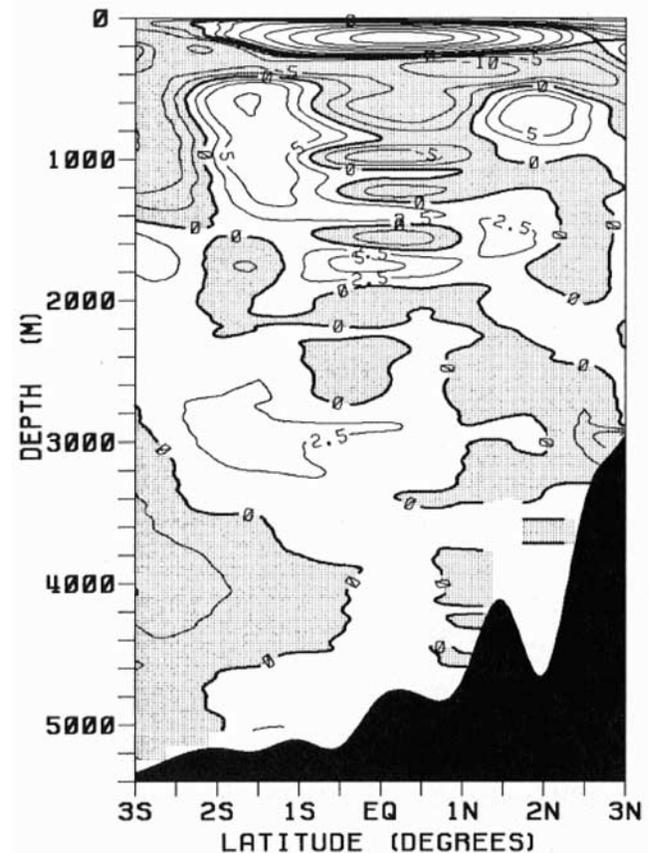
Figure 9. Observation of vertically stacked zonal jets near the equator, based on 16 months of observations. The average zonal flow is shown. Westward flow is shaded. Contours are on integral multiples of 10 cm s^{-1}, and there are additional contours at ±2.5 and ±5 cm s^{-1}. From *Firing* [1987]. Reprinted with permission.

employing a stability argument, was proposed by *Hua et al.* [1997], following the analysis by *Emanuel* [1979] on mesoscale convective systems in the atmosphere. Both considered an equatorial zonal jet $\bar{u}$, uniform in the zonal direction, and examined the instability problem. So-called inertial instabilities can arise if $fQ_E \leq 0$, where Q_E is the Ertel potential vorticity, which depends on the stratification, the Coriolis parameters f and $\tilde{f}$, and the meridional and vertical shear of $\bar{u}$. Analytical and numerical results by *Hua et al.* [1997] show that the instability manifests itself as a stacked structure of equatorial zonal jets. Later observations possibly confirm this mechanism [*Send et al.*, 2002; *Bourlès et al.*, 2003]; the condition for instability, at least, is fulfilled. The specific role (and importance) of $\tilde{f}$ in this mechanism has not yet been clarified.

[42] We note that the deep jets are actually more complex than Figure 9 might suggest. *Dengler and Quadfasel* [2002] showed that they also involve significant meridional currents and, moreover, vary considerably in time. One may speculate that the deep jets are in some way linked to the deep western boundary current, for *Richardson and Fratantoni* [1999] found that floats sometimes follow this deep current across the equator but are at other times carried eastward parallel to the equator, typically between $2°$ and $4°$N/S, while floats in the immediate vicinity of the equator are carried westward. In numerical model calculations, *d'Orgeville et al.* [2007] found that oscillations in the western boundary current may provoke mixed Rossby-gravity waves, whose instability subsequently leads to equatorial deep jets. An alternative line of explanation was pursued by *Dengler and Quadfasel* [2002], who showed that an interpretation in terms of (traditional) equatorial Rossby waves fits the data on deep jets reasonably well. Still another hypothesis on the origin of deep jets, namely, the development of mean flows by internal wave focusing, is discussed in section 6.2.2.

[43] We finally note that stacked equatorial jets have equally been observed in the mesosphere at heights of around 50 km. Following *Hua et al.* [1997], *Fruman* [2005] developed a theory for the atmospheric case and found from the stability analysis that $\tilde{f}$ makes the basic jet more unstable. This underlines the importance of abandoning the TA in the equatorial region.

6. INTERNAL WAVES

[44] Internal waves are oscillatory motions whose largest amplitudes occur in the interior of the fluid; they are an ubiquitous phenomenon in the oceans and atmosphere. Here buoyancy and the Coriolis force act as the restoring forces. This lends a key role to the three parameters associated with these forces: the buoyancy frequency N (being a measure of the density stratification), the Earth's angular velocity Ω, and latitude ϕ. The buoyancy frequency is defined as

$$N^2 = -\frac{g}{\rho_0}\left(\frac{d\rho_0}{dz} + \frac{\rho_0 g}{c_s^2}\right). \qquad (21)$$

[45] Here c_s is the speed of sound, and $\rho_0(z)$ is the static in situ density field. (Under the Boussinesq approximation, the ρ_0 in the denominator is replaced with a constant reference value of density, ρ_*.) For buoyancy (gravity) to act as a restoring force, the fluid must be stably stratified, i.e., $N^2 > 0$. In the lower atmosphere, values range from 0.01 (troposphere) to 0.02 rad s^{-1} (stratosphere). In the ocean, values of N can be as high as 10^{-2} rad s^{-1} (seasonal thermocline), but they are much lower in the deep ocean, typically in the range 3×10^{-4} to 2×10^{-3} rad s^{-1}. An example is shown in Figure 10 for a latitudinal section; here N is scaled with 2Ω. We note that the condition $N \gg 2\Omega$ (on which the TA implicitly hinges, as will be discussed below) is not satisfied in the deepest layers of the ocean.

[46] In the atmosphere, internal waves are particularly important in relatively strongly stratified layers such as the stratosphere [*Fritts and Alexander*, 2003]. In the ocean, they have vertical amplitudes as large as tens, or even hundreds, of meters and periods that range, roughly, from minutes to days. However, most of their energy is contained at low frequencies, especially at the tidal and near-inertial frequencies. In recent years, much attention has been paid to their role in (deep) ocean mixing [see, e.g., *Garrett and St. Laurent*, 2002].

[47] The significance of the parameters N (regarded as a constant for the moment), Ω, and ϕ to the dynamics of internal waves can be most easily appreciated by looking at the range of allowable frequencies. Internal waves of a given frequency do not necessarily exist at all latitudes; propagating poleward, they may encounter a "turning" or "critical" latitude ϕ_c, beyond which they cannot propagate as a free wave. An expression for ϕ_c was derived by *Hughes* [1964] [see also *LeBlond and Mysak*, 1978]:

$$\phi_c = \pm \arcsin\left[\frac{\omega^2}{4\Omega^2} - \frac{\omega^2}{N^2}\left(\frac{\omega^2}{4\Omega^2} - 1\right)\right]^{1/2}, \qquad (22)$$

where ω is the internal wave frequency; the plus (minus) sign applies to the Northern (Southern) Hemisphere. This expression is based on the full Coriolis force. Making the TA amounts to taking $N \to \infty$ in (22), so that the turning latitude shifts to the inertial latitude, i.e., the latitude at which the wave frequency equals the inertial frequency $|f|$:

$$\phi_i = \pm \arcsin\left(\frac{\omega}{2\Omega}\right). \qquad (23)$$

The distance between the "nontraditional" critical latitude (22) and the "traditional" version (23) is very substantial in the weakly stratified abyssal ocean, as is illustrated in Figure 19 (discussed in section 6.2.1); near-inertial waves can propagate much farther poleward in the former case.

[48] For weak stratification, the difference between the two is further illustrated in Figure 11, where stratification increases from zero (Figure 11a) to 4Ω (Figure 11d). The former value is representative of convective layers; the latter is found in the deepest parts of the ocean (dark blue regions in Figure 10). The grey area indicates the range of internal
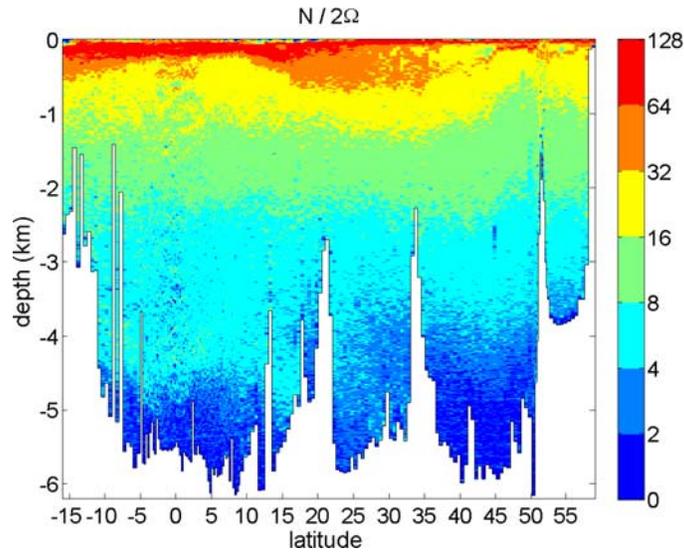
Figure 10. Relative strength of stratification, $N/2\Omega$, derived from temperature and salinity profiles in the Pacific Ocean for a south-north section near 179°E (WOCE section P14 from the Fiji Islands to the Bering Sea). These profiles were used to calculate, via the equation of state for the Gibbs potential, in situ density ρ_0 and the speed of sound c_s, and hence $N^2 = g^2(d\rho_0/dp - c_s^{-2})$, being equivalent to (21). Smoothing was applied by taking the running mean over 15 pressure levels (∼30 m); incidental points where $N^2 < 0$ were then set to zero. Note the logarithmic color scaling. In the deepest layers (dark blue), the ratio $N/2\Omega$ is fairly low; here nontraditional effects can be expected to significantly affect internal wave dynamics; the same applies to the upper mixed layer.
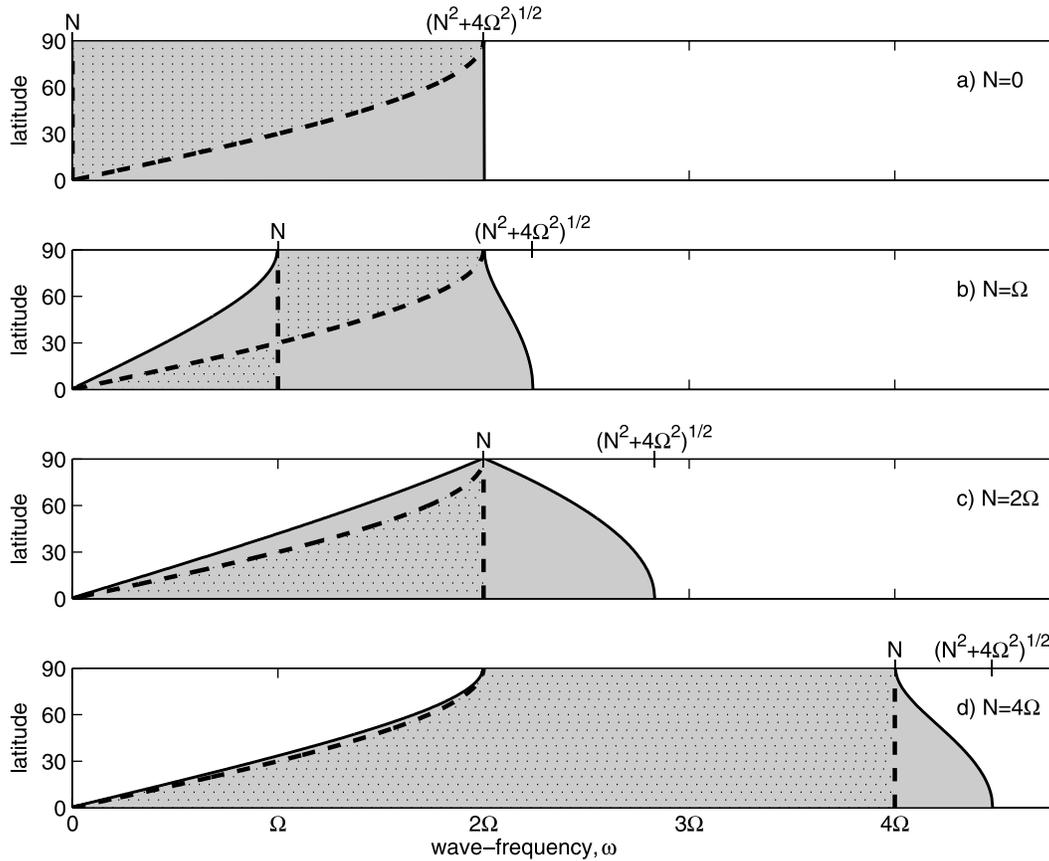
Figure 11. Internal wave frequency range as a function of latitude, stratification increasing from (a) $N = 0$, (b) $N = \Omega$, (c) $N = 2\Omega$, to (d) $N = 4\Omega$. The boundaries of the range (depicted in grey) are indicated by solid curves, representing (22). For comparison, the range as obtained under the TA is also shown (dashed lines and dotted regions).

wave frequencies, being enclosed by the solid curves calculated from (22). In Figures 11a–11d, the range under the TA is shown as well (dotted region), enclosed by the inertial latitude ϕ_i at one side (the dashed curve, being the same in all plots since ϕ_i is independent of stratification) and by N (vertical dashed line) at the other side. Figure 11 clearly demonstrates that the TA reduces the range of allowable frequencies at all latitudes (except the poles). Furthermore, it either introduces a turning latitude where none exists if the TA is not made (Figures 11a and 11b) or shifts it to the lower, inertial latitude (Figures 11b–11d).

[49] In Figure 11a, gravity cannot act as a restoring force because $N = 0$, leaving the Coriolis force as the sole restoring force. Internal waves are then usually referred to as gyroscopic or inertial waves. The latter term is not to be confused with the so-called inertia oscillation, a circular oscillation strictly at $\omega = |f|$; for this reason, we shall adopt the former term, following *Tolstoy* [1963] and *LeBlond and Mysak* [1978]. Overall, the allowable frequencies of gyroscopic waves cover the whole range from zero to 2Ω. They can exist at all latitudes if the TA is not made (grey area in Figure 11a); the TA reduces their habitat to the region poleward of the inertial latitude (i.e., above the dashed curve).

[50] In sections 6.1 and 6.2, we consider the effect of the TA on internal waves in more detail, with increasing geometric complexity. The simplest approach is to assume that the whole dynamics takes place at a fixed latitude (f plane); one key result here is the existence of a low-frequency short-wave limit, which disappears under the TA. In reality, of course, waves propagating in the meridional direction undergo a variation in latitude, a particularly important effect for waves having a frequency close to $|f|$ (near-inertial waves). To a first approximation, this effect can be included by using the β plane. One can then study what happens when a near-inertial wave approaches its turning latitude. A key result, discussed in section 6.2.1, is that in spite of its name, internal wave energy may accumulate at the "turning" latitude; this effect disappears under the TA.

[51] A still higher degree of complexity arises when one considers a thick spherical shell, as is usually necessary in the case of giant planets and rotating stars, or the Earth's liquid outer core. The metric terms then come fully into effect, accounting for the different curvature of concentric shells. Moreover, the variation of gravity g with radial distance needs to be included. This modifies N in (21); for example, if one regards the part in brackets as a constant, then N^2 still varies linearly with radius r via g. This leads to a modification of the picture presented in Figure 11, where N was assumed constant; there the turning latitude (belonging to a given wave frequency) was the same throughout the water column. In the general case of a (thick) spherical shell, a dependence on depth arises. Specifically, *Friedlander and Siegmann* [1982] and *Dintrans et al.* [1999], using the full Coriolis force throughout, introduced a classification by distinguishing $\omega < 2\Omega$ and $\omega > 2\Omega$; in the

former case, the turning surfaces are of hyperboloidal shape ("H modes"); in the latter, they are ellipsoidal ("E modes"). A further distinction is made between $\omega < N$ (H$_2$ and E$_1$) and $\omega > N$ (H$_1$ and E$_2$). These modes, of course, also appear in Figure 11, even though the curvature of the turning surfaces is extinguished by the implicit assumption of a thin shell. For example, in Figure 11a, there are only H$_1$ modes, while in Figure 11d, there are three modes: H$_2$ ($\omega < 2\Omega$), E$_1$ ($2\Omega < \omega < N$), and E$_2$ modes ($N < \omega < (N^2 + 4\Omega^2)^{1/2}$). However, in the terrestrial case, the ellipsoidal turning surface E$_1$ lies inside the "solid" Earth, and for this reason no turning latitude is found in that regime unlike for E$_2$.

6.1. Internal Waves on the (Nontraditional) f Plane

[52] For later reference, we start with a concise overview of the linear internal wave theory on the "nontraditional" f plane, bringing together elements that are somewhat scattered in the literature [*Tolstoy*, 1963; *O. M. Phillips*, 1966; *Saint-Guily*, 1970; *LeBlond and Mysak*, 1978; *Brekhovskikh and Goncharov*, 1994; *Miropol'sky*, 2001].

6.1.1. Summary of Linear Internal Wave Theory

[53] The momentum equations (8–10) are used with $\beta = 0$. The advective terms are neglected as we assume wave amplitudes to be infinitesimal (linear theory). Together with the continuity and energy equations (under the Boussinesq approximation), wave solutions of the form exp $i\omega t$ (with wave frequency $\omega > 0$) are then found to be governed by

$$A_* \frac{\partial^2 w}{\partial y^2} + 2B_* \frac{\partial^2 w}{\partial y \partial z} + C \frac{\partial^2 w}{\partial z^2} + D \frac{\partial^2 w}{\partial x^2} = 0 \qquad (24)$$

where $A_* = N^2 - \omega^2 + \tilde{f}^2$, $B_* = \tilde{f}f$, $C = f^2 - \omega^2$, and $D = N^2 - \omega^2$. The presence of $\tilde{f}$ has two important consequences. First, it introduces a mixed derivative (the term with B_*), thereby changing the character of the partial differential equation; second, it makes the roles of x and y dissimilar (since $B_* \neq 0$ and $A_* \neq D$), implying anisotropy in the horizontal plane. Both effects disappear under the TA. Strong stratification ($N \gg 2\Omega$) diminishes the role of $\tilde{f}$ in A_* but does not affect the presence of the mixed derivative. *Phillips* [1968] already pointed out that $\tilde{f}$ "may enter significantly in the finer details" even when $N \gg 2\Omega$. As will become clear in sections 6.1.2 and 6.2, "finer" can be taken literally here: short-scale wave patterns arise at subinertial frequencies (i.e., lower than $|f|$) that wholly disappear under the TA.

[54] Assuming plane waves traveling in a direction α north of east, i.e., along the direction of increasing $\chi = x\cos\alpha + y\sin\alpha$, (24) reduces to

$$A \frac{\partial^2 w}{\partial \chi^2} + 2B \frac{\partial^2 w}{\partial \chi \partial z} + C \frac{\partial^2 w}{\partial z^2} = 0, \qquad (25)$$

with $A = N^2 - \omega^2 + f_s^2$ and $B = ff_s$; here $f_s = \tilde{f}\sin\alpha$. For wave propagation to be possible, hyperbolicity is required,
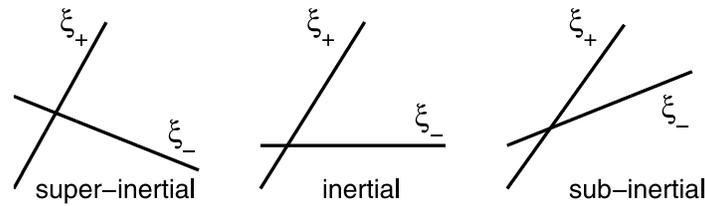
Figure 12. An example of "nontraditional" characteristics, showing the direction of energy propagation in the meridional/vertical plane (poleward to the right) for the regime $|f| < (N^2 + f_s^2)^{1/2}$. Three different cases are shown (left to right): $|f| < \omega < (N^2 + f_s^2)^{1/2}$, $\omega = |f|$, and $\omega < |f|$. Note the change in orientation of the characteristic ξ_- as it goes from superinertial to subinertial. Under the TA (not shown), only the superinertial case would exist, with then ξ_+ and ξ_- of equal steepness. From *Gerkema and Shrira* [2005b]. Reprinted by permission from Cambridge University Press.

i.e., $B^2 - AC > 0$; this inequality provides the upper and lower bounds of the frequency domain of internal waves:

$$\omega_{min,max} = \frac{1}{\sqrt{2}}$$
$$\cdot \left\{ \left(N^2 + f^2 + f_s^2\right) \mp \left[\left(N^2 + f^2 + f_s^2\right)^2 - (2fN)^2\right]^{1/2} \right\}^{1/2}. \tag{26}$$

For meridional propagation ($\alpha = \pi/2$), we have $f^2 + f_s^2 = 4\Omega^2$. Equation (26) can then be rewritten such that ϕ is expressed in terms of the frequencies ω, Ω, and N; this yields the critical latitude ϕ_c already mentioned in (22): the extremes of the frequency domain are reached precisely at ϕ_c (Figure 11). For zonal propagation ($\alpha = 0$), on the other hand, the upper and lower bounds (26) become identical to those found under the TA, namely, $\min\{|f|, N\} < \omega < \max\{|f|, N\}$.

[55]   For a strongly stratified fluid ($N \gg 2\Omega$), (26) can be approximated by

$$\omega_{min} = |f| \left[1 - \frac{f_s^2}{2N^2} + O\left(\frac{\Omega^4}{N^4}\right)\right];$$
$$\omega_{max} = N \left[1 + \frac{f_s^2}{2N^2} + O\left(\frac{\Omega^4}{N^4}\right)\right],$$

where the last term in each equation represents the order of magnitude (O) of the higher-order terms. Thus, in this limit, the lower and upper bounds approach the traditional values. However, as illustrated in Figure 10, the condition $N \gg 2\Omega$ is not satisfied in the deeper layers of the ocean, and here nontraditional effects can be expected to be important.

[56]   There are two main roads to solve (25). For constant stratification ($N = $ const), all coefficients are constant, and the general solution can be written

$$w = F(\xi_+) + G(\xi_-), \tag{27}$$

where F and G are arbitrary functions and $\xi_\pm = \mu_\pm \chi - z$ are the characteristic coordinates, with

$$\mu_\pm = \frac{B \pm (B^2 - AC)^{1/2}}{A}. \tag{28}$$

Internal wave energy propagates along the characteristics $\xi_+ = $ const or $\xi_- = $ const; examples are sketched in Figure 12 for different frequency regimes.

[57]   The dispersion relation can be derived by substituting $w = \exp i(k\chi + mz)$ in (25). Writing the wave vector as $(k, m) = \kappa(\cos\theta, \sin\theta)$ then gives the dispersion relation

$$\omega^2 = N^2 \cos^2\theta + (f_s \cos\theta + f \sin\theta)^2. \tag{29}$$

As under the TA, the wave frequency depends on the direction θ of the wave vector but not on its length κ, which implies that the group velocity vector ($\partial\omega/\partial k$, $\partial\omega/\partial m$) must be perpendicular to the wave vector, as is illustrated in Figure 13 for gyroscopic waves. (This is borne out by the identity $\mu_\pm = -\cot\theta$, which follows from (29).) For the fully three-dimensional case (24), the dispersion relation is discussed by *LeBlond and Mysak* [1978], in which case, surfaces of constant wave frequency are cone-like. Here, too, the dispersion relation leaves the magnitude of the wave number (κ) undetermined; an external length scale needs to be introduced to specify wave numbers. The size of a body force may serve this purpose. Notice also that the relations derived so far implicitly assume a medium of infinite extension. Once one introduces a horizontal bottom and surface (and hence the external scale, water depth), a discrete set of wave numbers appears with specific length scales, as, for example, in (32).

[58]   So far, we assumed N to be constant. If N varies with the vertical z, (27) no longer provides a solution. The underlying reason is that the inhomogeneity of the medium causes internal reflections, so the wave energy no longer stays on the same characteristic in the interior of the fluid. However, if the fluid is contained between two horizontal boundaries (an even bottom below and a "rigid lid" above), a solution may be obtained in terms of vertical modes for arbitrary $N(z)$. These modes W_n, with mode number n, are found by substituting

$$w = W(z) \exp ik(\chi - Bz/C) \tag{30}$$

into (25), which yields

$$\frac{d^2 W}{dz^2} + k^2 \left[\frac{B^2 - AC}{C^2}\right] W = 0. \tag{31}$$
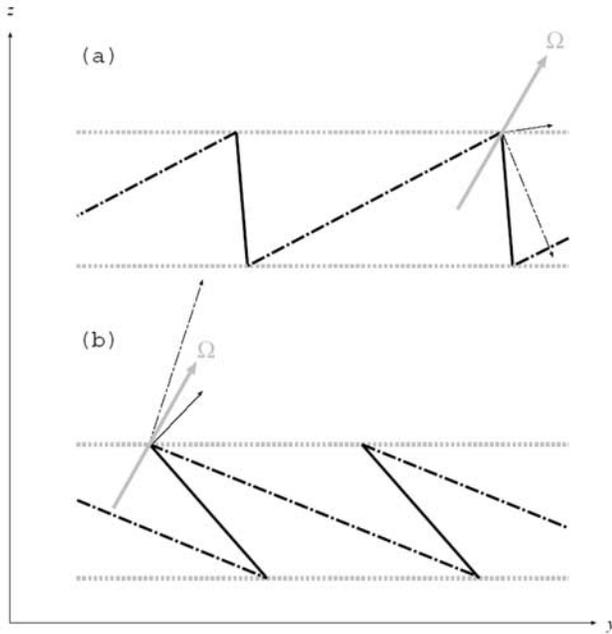
Figure 13. Characteristics for gyroscopic waves ($N = 0$) in a vertically confined basin for (a) subinertial frequencies ($\omega < |f|$) and (b) superinertial frequencies ($\omega > |f|$). Here, energy propagates upward along solid lines and downward along dotted-dashed lines. The direction of phase propagation, which is perpendicular to energy propagation, is indicated by solid and dotted-dashed arrows, respectively. The TA is not made, so the rotation vector Ω is not aligned to the vertical. Under the TA, only the case in Figure 13a would exist but then with symmetric propagation with respect to the vertical. From *Durran and Bretherton* [2004].

Together with the boundary conditions $W = 0$ at $z = -H, 0$ (bottom and surface), this constitutes a Sturm-Liouville problem. Its solution is formed by a set of eigenvalues k_n and corresponding eigenfunctions W_n, whose form depends, of course, on $N(z)$. Importantly, (30) contains two types of z dependences, unlike under the TA, where $B = 0$. Indeed, the nonseparable nature of the solution, due to the presence of the mixed derivative, becomes apparent if one takes the real part of (30).

6.1.2. Properties of Internal Inertiogravity Waves

[59] In the ocean and lower atmosphere, one generally has $N > 2\Omega$. Under the TA, the lower bound of the frequency range is then $|f|$. In the "nontraditional" equation (26), by contrast, the lower bound lies slightly below $|f|$ (see also Figure 11d). So there is a class of subinertial internal inertiogravity waves ($\omega_{min} < \omega < |f|$), which wholly disappears under the TA. They were examined in the oceanic context [*Saint-Guily*, 1970; *Badulin et al.*, 1991; *Brekhovskikh and Goncharov*, 1994; *Gerkema and Shrira*, 2005b] and recently also in the atmospheric context [*Thuburn et al.*, 2002b; *Kasahara*, 2003a, 2003b, 2004; *Durran and Bretherton*, 2004]. This class of waves appears under various names in the literature; *Durran and Bretherton* [2004] rightly emphasized that despite the distinctive properties of these waves, the restoring forces

at work are just buoyancy and rotation (possibly combined with elastic forces in compressible fluids) and that they can exist in the absence of boundaries; in these respects, they are no different from traditional internal inertiogravity waves.

[60] There are two possible regimes, depending on which of the two, $|f|$ or $(N^2 + f_s^2)^{1/2}$, is the largest. For the regime $|f| < (N^2 + f_s^2)^{1/2}$, the dispersion relation (29) is shown in Figure 14a. Segments where the frequency increases (decreases) as a function of θ correspond to propagation along a μ_+ (μ_-) characteristic. The wave vector and group velocity vector are either vertically or horizontally opposed but not both (Figures 14b and 14c). In Figure 14a, dotted lines are drawn at two frequency levels: $\omega = (N^2 + f_s^2)^{1/2}$ and $\omega = |f|$; these are precisely the values at which the coefficients A and C in (25) change sign, respectively. Their special significance is furthermore seen from the simple rule that one can distill from Figure 14: for the μ_+ characteristic, the wave vector and group velocity are vertically opposed for $\omega_{min} < \omega < (N^2 + f_s^2)^{1/2}$ and horizontally opposed for $(N^2 + f_s^2)^{1/2} < \omega < \omega_{max}$; for the μ_- characteristic, they are vertically opposed for $|f| < \omega < \omega_{max}$ and horizontally opposed for $\omega_{min} < \omega < |f|$. A similar kind of rule can be derived for the other regime, $(N^2 + f_s^2)^{1/2} < |f|$. This variety of behavior is to be contrasted with the traditional limit ($f_s = 0$), where one finds that they are always vertically opposed in the "strongly" stratified regime (i.e., $|f| < N$) and always horizontally opposed in the "weakly" stratified regime ($N < |f|$).

[61] In a vertically bounded domain, energy needs to propagate both upward and downward, and this results in a combined role of the characteristics, one taking over from the other at the boundaries. (An example for $N = 0$, i.e., gyroscopic waves, is shown in Figure 13.) One can alternatively obtain a solution in terms of modes from (31). For constant N, this yields the following dispersion relation:

$$k_n = \frac{\pm(n\pi/H)(\omega^2 - f^2)}{\left[(\omega^2 - \omega_{min}^2)(\omega_{max}^2 - \omega^2)\right]^{1/2}}. \tag{32}$$

This relation, as well as that of the horizontal component of the group velocity, is shown in Figure 15. As usual, waves become short at the upper bound ω_{max}. Importantly, here they also become short at the lower bound ω_{min}; we refer to this phenomenon as the subinertial short-wave limit. It affects not only the horizontal scale but also the vertical one via the second vertical dependence in (30). This subinertial short-wave limit is present no matter how strong the stratification is, but it disappears under the TA; in this sense, the TA has the character of a singular limit. Another important feature is the smooth passage through $|f|$ (see Figure 15); such a transition occurs when low-frequency waves move to higher latitudes, so that $|f|$ increases, and the waves may turn from superinertial into subinertial. This is discussed in section 6.2.1.

[62] For variable $N(z)$, another property of subinertial waves emerges. *Brekhovskikh and Goncharov* [1994] noted that their habitat lies in weakly stratified regions; for a given
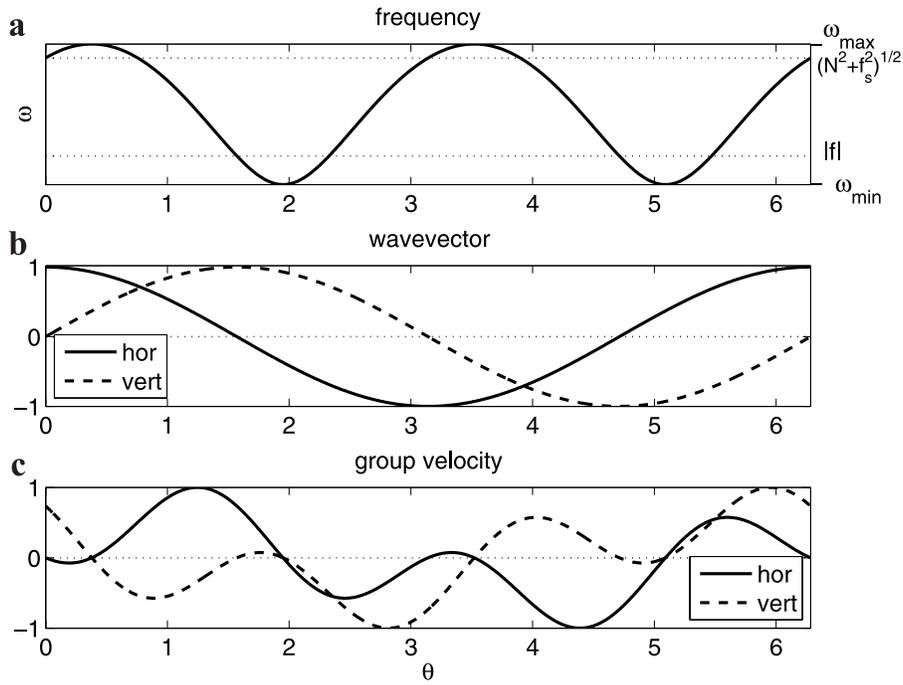
Figure 14. Dispersion relation (29) for internal inertiogravity and related quantities for the regime $|f| < (N^2 + f_s^2)^{1/2}$. (a) Wave frequency versus θ, the angle of the wave vector with the horizontal. Segments where ω increases (decreases) correspond to the characteristic μ_+ (μ_-). (b) Horizontal and vertical components of the wavevector (normalized), also as a function of θ. (c) Components of the group velocity factor (multiplied by ω and normalized). Parameter values are $\phi = 45°N$ and $\alpha = \pi/2$; for optimal clarity, N has been chosen to be only marginally larger than 2Ω ($N = 1.5 \times 10^{-4}$ rad s^{-1}).

subinertial wave frequency, stratification needs to be sufficiently weak for them to exist, a consequence of (26). For example, with N^2 linearly decreasing downward with z, the subinertial vertical modes can be solved from (31) in terms of Airy functions, which are oscillating in the deepest part of the water column and fall off exponentially above it, where stratification is higher. They are thus trapped in the weakly stratified abyss (Figure 16).

[63] The results presented here demonstrate clearly that abandoning the TA does not pose any mathematical hurdle as long as we consider internal waves on the (nontraditional) f plane. The theory can be extended to the treatment of internal wave reflection from sloping boundaries [*Gerkema and Shrira*, 2006; *Gerkema*, 2006]. For nontraditional effects in critical layer absorption, see *Grimshaw* [1975a]. There have been some "nontraditional" numerical studies on internal waves [*Beckmann and Diebels*, 1994; *Kasahara and Gary*, 2006], illustrating the properties discussed above. *Baines and Miles* [2000] recommend that the horizontal component $\tilde{f}$ be included in internal tide generation models; they found that the component causes a small increase in the conversion rate from barotropic to baroclinic tidal energy, as well as a change in the paths of energy propagation. Both features are illustrated for a realistic setting in Figure 17, based on recent numerical model calculations.

6.1.3. Observations

[64] Current measurements in the ocean provide information on the polarization of the horizontal velocity field. From the general expressions of *Gerkema and Shrira*

[2006], one can derive the following relation for plane waves propagating at an angle α with respect to the east:

$$|v'|/|u'| = |(f_s\mu_\pm - f)/\omega|. \tag{33}$$
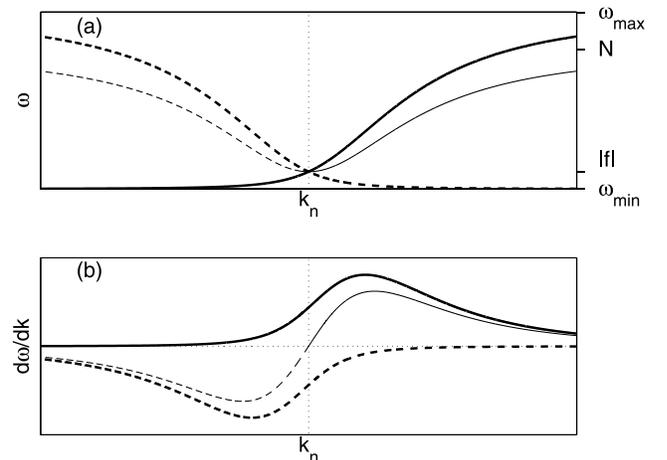
Figure 15. Dispersion relation in a vertically bounded system, equation (32), for plus and minus signs (solid and dashed lines, respectively). (a) Wave frequency as a function of the horizontal wave number k_n. (b) Horizontal component of the group velocity. Thick lines represent the nontraditional dispersion relation; thin lines represent dispersion under the TA ($f_s = 0$). Horizontal and vertical dotted lines represent zero axes. After *Gerkema and Shrira* [2005b]. Reprinted by permission from Cambridge University Press.
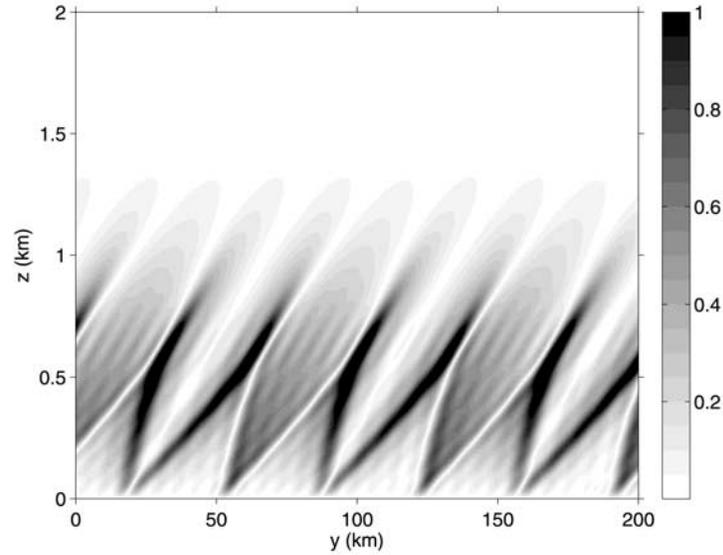
Figure 16.   An example in which the buoyancy frequency N decreases in the downward direction, mimicking the slow decrease of N with depth in the abyssal ocean. Subinertial modes are now trapped in the region of weakest stratification. The amplitude of the vertical velocity is shown (subject to an arbitrary scale factor) for a superposition of five modes. From *Gerkema and Shrira* [2005b]. Reprinted by permission from Cambridge University Press.

Here $|u'|$ denotes the amplitude of the velocity in the direction of wave propagation, and $|v'|$ denotes the amplitude of the velocity in the perpendicular direction. Unlike under the TA, the polarization is not the same for the characteristics μ_+ and μ_-. For example, at the inertial frequency $\omega = |f|$, the μ_- corresponds to circular polarization (as under TA), but μ_+ corresponds to an ellipse-like polarization, whose eccentricity depends on stratification N. An interesting test case for (33) is the observation in the Mediterranean by *van Haren and Millot* [2004]; they bandpass filtered their current meter data around f; see Figures 18b and 18c. Although the stratification varies with time (see especially the change in the "steps" above 1500 m), the ambience of the upper current meter at 1800 m was significantly stratified throughout ($N \approx 2\text{–}3 \; f$), while stratification was extremely weak at 2700 m ($N \approx 0\text{–}0.4f$), where the lower current meter was placed. Vertical propagation of near-inertial energy can occur only via the ξ_+ characteristic (see Figure 12 (middle)), so we use μ_+ in (33). One then finds that in the stratified layer at 1800 m, theory predicts a ratio of major to minor axis between 1.24 and 1.34. (The error range stems from the dependence on the horizontal direction of wave propagation α, which can only approximately be inferred from the observations.) The observed value derived from Figure 18b lies between 1.25 and 1.5 in good agreement with the theoretical range. The ratio is much larger in the near-homogeneous layer at 2700 m (Figure 18c): 3.2–4.2 (theory) against the observed value of 2–3.5. Another nontraditional effect is the occurrence of a significant vertical velocity component at near-inertial frequencies, which has also been observed [*van Haren and Millot*, 2005].

[65]   The coexistence of nearly unstratified layers ($N \ll 2\Omega$) with significantly stratified ones, as, for example, in Figure 18a, raises the question of whether they may act as waveguides for internal waves of a given frequency. The answer depends strongly on whether one makes the TA or not [*van Haren*, 2006]. Under the TA, there is no overlap at all between the frequency range for gyroscopic waves occurring for $N = 0$, i.e., $0 < \omega < |f|$, and that for inertiogravity waves in layers with $N > |f|$, i.e., $|f| < \omega < N$. In other words, internal waves existing in one layer cannot penetrate the other layer. By contrast, if one abandons the TA, an overlap between the regimes exists, which covers at least a range of near-inertial frequencies (see Figures 11a and 11d). The very existence of near-inertial waves in both layers, as demonstrated in Figures 18b and 18c, thus lends support to the "nontraditional" theory. The transition between gyroscopic and inertiogravity waves is important in the astrophysical context as well; see section 7.1.

[66]   We note that near-inertial waves seem to undergo a change in polarization (from predominantly circular to rectilinear) within a narrow band across the equator [*van Haren*, 2005]; one would expect this to be due to nontraditional effects, but (33) does not, in fact, predict such a transition. Possibly a more complete description, including the equatorial β effect, is needed to explain the observed features, but this has not yet been examined.

6.2.   Internal Waves Subject to Latitudinal Variation

[67]   Section 6.1.2 makes clear that the lower bound $\omega_{\min}$ acts as a short-wave limit if the TA is abandoned. One can therefore expect a short-wave singularity to occur at the turning latitude, and this is indeed a recurring theme in the remainder of this section.
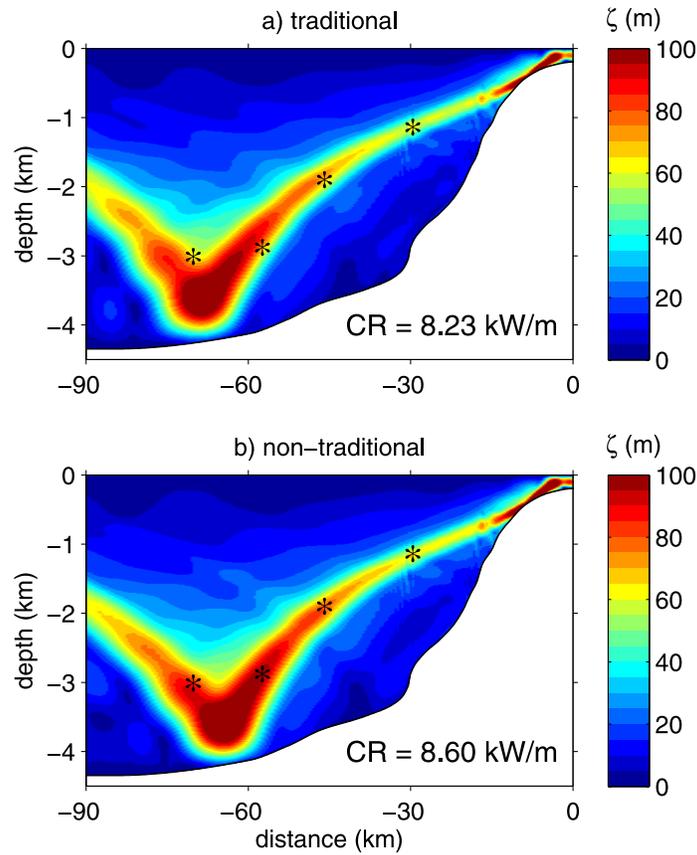
Figure 17. Amplitudes of isopycnal excursions ζ (in m) from a linear internal tide generation model, using observed stratification and topography (Bay of Biscay). (a) Original model, described by *Gerkema et al.* [2004], hydrostatic and using the TA. (b) Inclusion of nontraditional terms, giving a quasi-hydrostatic version. In both plots, the asterisks show at what depth maximum excursions occur according to in situ observations by *Pingree and New* [1991]. Overall, the nontraditional model run gives a better correspondence with these observations, the downgoing beam originating from the shelf break being steeper and the bottom-reflected one being less steep than under the TA. The conversion rate (CR), or energy flux, is increased by nontraditional effects by 4.5%.

6.2.1. Propagation on the β Plane

[68] Latitudinal variation of the Coriolis parameter f is important to near-inertial waves, even though their horizontal length scales are fairly small compared to the radius of the Earth. The reason is that they may over a short distance turn from superinertial to subinertial or vice versa. To describe these effects in the simplest possible way, one adopts the β plane as described in section 2.2; here $f = f_0 + \beta y$ varies linearly with the meridional coordinate y, while $\tilde{f}$ is taken to be constant. Since nontraditional effects are strongest for propagation in the meridional direction, we examine only this case. The generalization of (25) then becomes

$$\left(N^2 - \omega^2 + \tilde{f}^2\right)\psi_{yy} + 2f\tilde{f}\psi_{yz} + \left(f^2 -; \omega^2\right)\psi_{zz} + \tilde{f}\beta\psi_z = 0, \quad (34)$$

[*Gerkema and Shrira*, 2005a] where we introduced the stream function ψ: $v = \psi_z$ and $w = -\psi y$. (For a more general version in terms of spherical coordinates, see *Needler and LeBlond* [1973]). Thus, the generalization from (25) into (34) consists simply in replacing the constant f in (25) by the y-dependent $f(y)$ in (34) and in adding one new term, the last one on the left-hand side of (34).

[69] Equation (34) can be simplified for certain regions. Near the equator, $f_0 \approx 0$ so that f can be replaced by βy throughout (section 6.2.2). For near-inertial waves propagating outside the near-equatorial band, on the other hand, we can make the following approximations. The variation with latitude matters here only because of the proximity of $|f|$ to wave frequency ω; apart from that, the β effect can be neglected. Now, the difference $|f| - \omega$ occurs only in one place in (34), namely, in the the factor $f^2 - \omega^2$, which we may approximate by $f_0^2 - \omega^2 + 2f_0\beta y$. Hence (34) becomes

$$A\psi_{yy} + 2B\psi_{yz} + (C + 2f_0\beta y)\psi_{zz} = 0, \quad (35)$$

with $A = N^2 - \omega^2 + \tilde{f}^2$, $B = f_0\tilde{f}$, and $C = f_0^2 - \omega^2$. Characteristics are now defined by

$$\frac{dz}{dy} = \frac{B \pm [B^2 - A(C + 2f_0\beta y)]^{1/2}}{A}.$$

Even though the medium is now inhomogeneous because of β, and possibly also because of $N(z)$, we will assume that these variations are sufficiently weak in the sense that
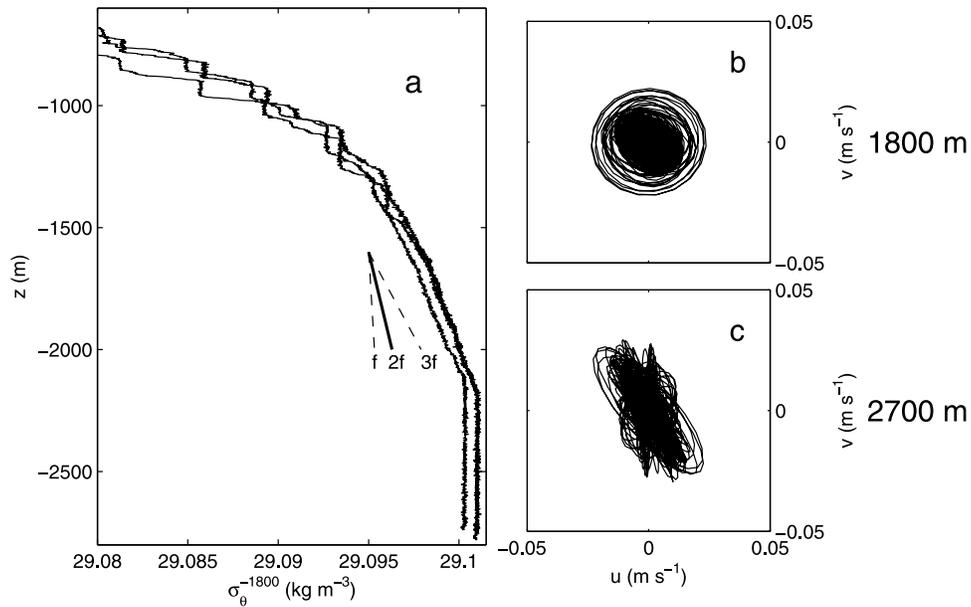
Figure 18. Observations from the Mediterranean. (a) Potential density profiles, showing a layer of very weak stratification below 2100 m. Hodographs based on near-inertial band-pass-filtered current meter data (u east and v north) at (b) 1800 m (where $N \approx 2.5 \times f$) and (c) 2700 m ($N \approx 0$). After *van Haren and Millot* [2004]. Reprinted by permission from Elsevier, copyright 2004.

internal wave energy propagates along the characteristics without the occurrence of any internal reflections (geometrical-optics approach). An example of such a propagation is shown in Figure 19, where the stratification follows an exponential profile, decreasing with depth. The wave energy enters the domain from the outer left, where the wave is slightly superinertial ($\omega > |f|$). As the wave propagates to the right, i.e., poleward, the Coriolis parameter $|f|$ increases and at $y = 0$ becomes equal to the wave frequency ω. At this point, the inertial latitude, the wave reflects under the TA (thin line). However, with $\tilde{f}$ included (thick line), the wave can propagate beyond the inertial latitude and becomes subinertial. This gives rise to the two phenomena that were discussed in section 6.1.2: First, the more poleward the wave gets, and hence the more subinertial, the closer it stays to the bottom; this is because the subinertial wave can only exist in sufficiently weakly stratified regions. Second, the length scale becomes shorter, in which we recognize the subinertial short-wave limit that comes into effect as the wave frequency approaches its lower bound. These two elements are interesting in view of the important topic of deep-ocean mixing, but this aspect has not yet been fathomed, although *Walter et al.* [2005] speculated that they may help explain latitudinal variations in abyssal vertical diffusivities. In any case, the mechanism would result in an enhancement of near-inertial energy in the deepest parts of the water column, a phenomenon that has been observed in some internal wave spectra [*van Haren et al.*, 2002; *van Aken et al.*, 2005].

6.2.2. Near-Equatorial Region

[70] Not all waves are trapped at the turning surface though; part of them reflect back toward the equator and may enter the other hemisphere and approach the opposite turning surface. While reflecting from surface, bottom, and turning surfaces, the waves still focus their energy but now onto one or two limit cycles that are present around the equator in between the turning surfaces. These periodic orbits act as "wave attractors," on which wave energy accumulates regardless of the exact source location. The location of these wave attractors appears to have a fractal dependence on a lumped parameter containing wave frequency, stratification rate, rotation rate, and the fluid domain's aspect ratio [*Maas and Harlander*, 2007]. The trapping that was observed on the β plane (section 6.2.1), near the intersection of turning surface and bottom, can be considered as a special, degenerate case of a (point) wave attractor.

[71] Historically, the discovery of the equatorial wave attractor proceeded in a few steps, which were carried through without applying the TA. *Stern* [1963] examined the dynamics of a homogeneous fluid on a nontraditional equatorial β plane, which is governed by (34) with $N = 0$ and $f_0 = 0$. In terms of scaled coordinates, he arrived at a simplified version by exploiting the fact that the resulting equation can be factorized:

$$\left(\frac{\partial}{\partial y} - (\sigma - y)\frac{\partial}{\partial z} \right)\left(\frac{\partial}{\partial y} + (\sigma + y)\frac{\partial}{\partial z} \right)\psi = 0, \qquad (36)$$

where σ is a rescaled and dimensionless version of the wave frequency. Taking $Y = 4\,y\,\sigma$ and $Z = 2(2z - y^2 - \sigma^2)$ transforms (36) into the hyperbolic spatial wave equation $\psi_{YY} - \psi_{ZZ} = 0$ (employing the subscript-derivative notation), which is to be solved subject to the requirement of vanishing stream function at the boundary. As such, this problem is ill-posed; conditions under which it becomes
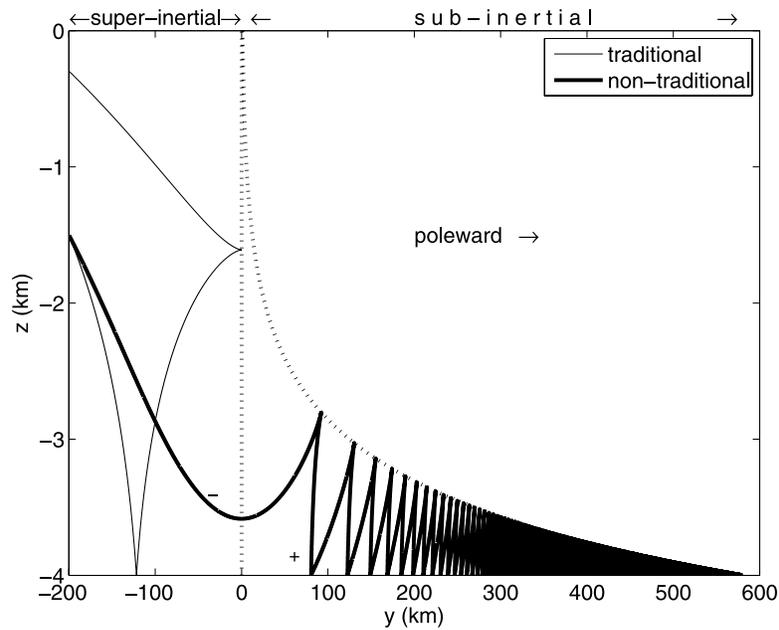
Figure 19. Characteristics showing the direction of energy propagation for near-inertial waves on the β plane. The stratification decreases exponentially downward: $N = N_0 \exp(z/b)$, with $N_0 = 5.24 \times 10^{-3}$ rad s^{-1} and $b = 1.3$ km, the standard Garrett-Munk profile. The coordinate y denotes the meridional direction (poleward to the right). The position $y = 0$ corresponds to latitude 45°N; a fixed wave frequency ω is chosen such that it equals f at $y = 0$. Since f increases poleward, waves are superinertial ($\omega > f$) for negative y and subinertial ($\omega < f$) for positive y. The transition between the two regimes occurs at $y = 0$, the inertial latitude. It acts as a turning latitude under the TA (thin solid line). In the nontraditional case (thick solid line), however, wave energy can propagate beyond the inertial latitude, so that the wave becomes subinertial; it then gets trapped in the weakly stratified abyss, its wavelength becoming progressively shorter as it further penetrates the waveguide. After *Gerkema and Shrira* [2005a].

well posed are described by *Maas and Harlander* [2007]. The general solution, in terms of the original coordinates, is formed by a superposition of the arbitrary functions $F[(y \pm \sigma)^2/2 - z]$. Stern deduced that the waves are equatorially trapped for some frequencies. *Bretherton* [1964] realized that Stern's solution might be related to the occurrence of certain closed raypaths for low-frequency internal (i.e., gyroscopic) waves in an unstratified spherical shell. These waves reflect from the boundaries while retaining their inclination relative to the rotation axis, and periodic paths were obtained for particular frequencies; examples are shown in Figure 20. This was indeed confirmed by *Stewartson* [1971, 1972a, 1972b], who showed that these periodic rays were actually attracting. *Israeli* [1972] subsequently showed that these wave attractors arose not just for special frequencies but over continuous frequency intervals. The occurrence of attractors is borne out by exact solutions of the Stern equation, an example of which is shown in Figure 21.

[72] Restoring stratification, the waves are spatially confined to reside within turning surfaces, across which the character of the governing differential equation changes from hyperbolic to elliptic [*Friedlander and Siegmann*, 1982]. *Dintrans et al.* [1999] observed that wave attractors are ubiquitous in this setting and that trapping may now also occur in the form of point attractors at the intersections of

turning surface and inner shell, an example of which was shown in Figure 19.

[73] The notion of a wave attractor is not specific to the equatorial shell per se. In fact, it arises in any geometry where reflecting boundaries break the symmetry imposed by the restoring forces [*Maas*, 2005]. As shown by (29), the frequency fixes the direction into which wave energy propagates, and only in oversymmetrized geometries (e.g., boundaries either parallel or perpendicular to net restoring direction) will the reflection of the wave be such that focusing (and defocusing) of wave rays can be avoided. It is exactly this oversymmetrization of the geometrical setting that the TA achieves by aligning the rotation axis to gravity. In doing so, it also simplifies the mathematical structure of the governing equation and boundary conditions by allowing separation of variables. In this way, only large-scale, regular standing wave structures arise. Dynamically, the significance of dropping the TA thus lies in breaking this reflectional symmetry [*Maas*, 2001]. But, it should be mentioned that abandoning the TA is merely one way of enforcing the solution to develop its generic behavior, characterized by dominance of wave focusing and the appearance of wave attractors with associated fine-scale structure. Adding "topography" provides another instance by which the reflectional symmetry is broken [*Maas and Lam*, 1995].
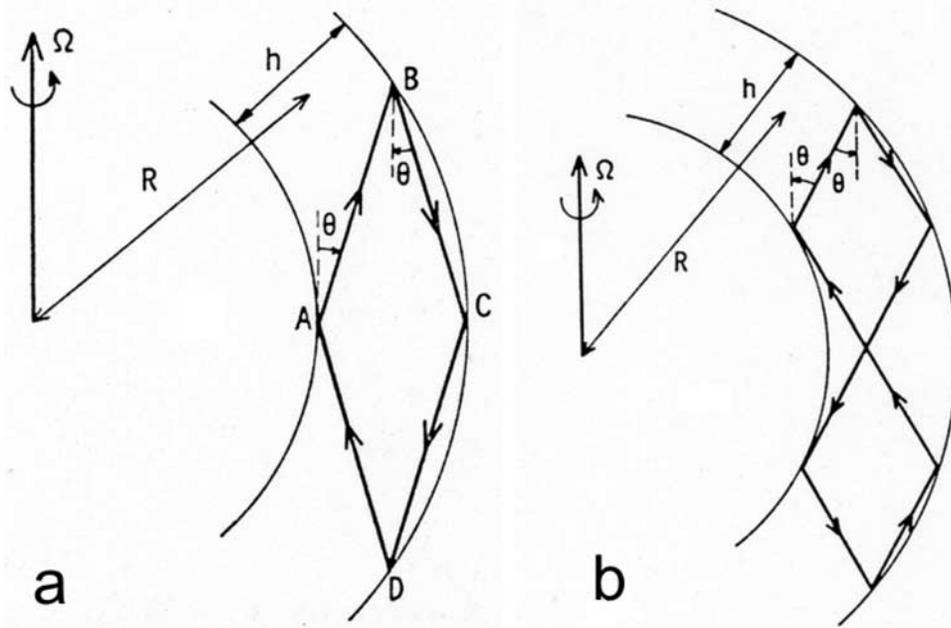
Figure 20. Examples of equatorially trapped gyroscopic waves in a spherical shell, illustrated by raypaths, along which their energy propagates. These patterns were later shown to act as wave attractors. From *Bretherton* [1964]. Reprinted by permission from Blackwell Publishing.

[74] On approaching the wave attractors, small-scale wave structures appear, which are susceptible to shear instabilities and may lead to mixing. In a laboratory experiment, *Maas* [2001] observed the development of a wave attractor in a periodically perturbed rotating homogeneous fluid, as illustrated in Figure 22a. (Here a sloping boundary provided the symmetry breaking instead of nontraditional effects.) A cyclonic mean flow coincided with its appearance (Figures 22b and 22c). This mean flow was present at all depths over the position where the internal wave attractor reflects from a sloping boundary and was attributed to the mixing of angular momentum that accompanies the internal wave focusing. *Maas* [2001] speculates that wave focusing onto an equatorial wave attractor may equally drive such a cyclonic mean flow, which may be partly responsible for the enigmatic equatorial deep jets discussed in section 5.3. In this explanation, the robustness of these jets is, on the one hand, due to the fact that wave attractors exist simply because of the geometry of the spherical shell in combination with the average stratification and Earth's rotation and, on the other hand, to their ability to continuously collect and amplify waves within the relevant frequency ranges from wherever these waves are generated within a particular equatorial belt.

[75] Meridional flows associated with equatorially trapped internal waves may have periods ranging from days to semiannual, as was analytically shown by *Raymond* [2000]; some of his wave solutions, moreover, were entirely dependent on the inclusion of $\tilde{f}$. Equatorial Kelvin waves (defined as having no meridional flow), too, are modified when the nontraditional Coriolis terms are taken into account. For a stratified fluid, *Raymond* [2001] showed that the usual Gaussian decay with meridional distance from the
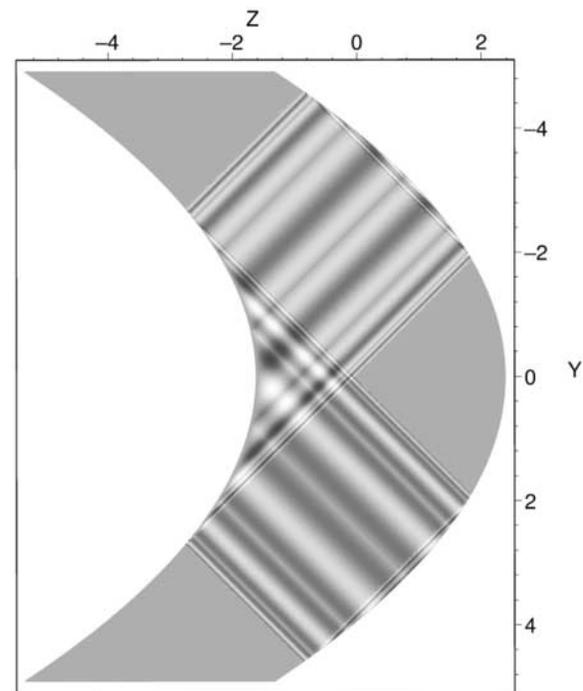
Figure 21. Example of an exact solution of the *Stern* [1963] equation (36), showing the stream function. This equation includes no stratification ($N = 0$). In the region inside the wave attractor, banded flow structures can be observed. The velocity is singular along the wave attractor. Here $\sigma = 0.9$; Y and Z are transformed coordinates. After *Harlander and Maas* [2006]. Reprinted with permission from E. Schweizerbart'sche Verlagsbuchhandlung, http://www.borntraeger-cramer.de/.
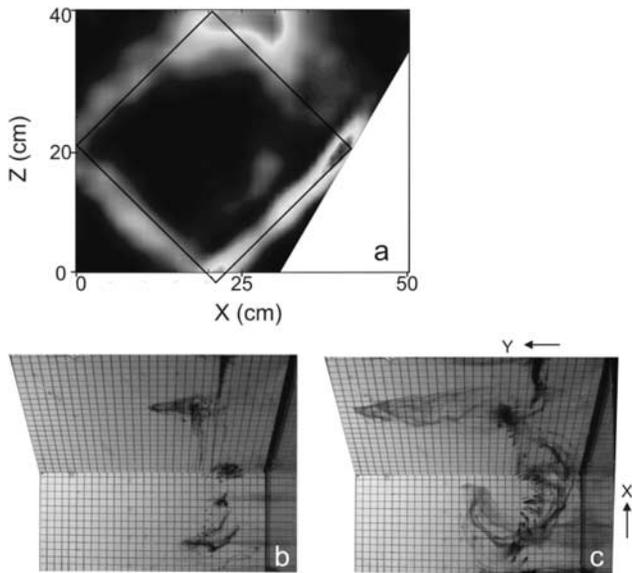
Figure 22. (a) Horizontal-vertical (x, z) distribution in a particular (y) cross section of the amplitude of a gyroscopic wavefield (white, high; black, small). The waves are excited in a homogeneous rotating fluid (rotation rate Ω) by weak modulation at frequency $\omega < 2\Omega$. It demonstrates the localization of wave energy at a wave attractor, whose predicted location is given by solid lines. Here the rotation axis is aligned to gravity, making the setting "traditional." However, the symmetry breaking that could otherwise be the result of nontraditional effects is caused here by a sloping bottom, giving rise to a wave attractor (Figure 22a) and a mean flow producing a dye distribution, seen from above (Figures 22b and 22c). (b) Initial distribution and (c) distribution after six wave periods. The sloping wall is located in the upper part. Strong leftward dye displacement occurs halfway over that slope, where the wave attractor reflects. From *Maas* [2001]. Reprinted by permission from Cambridge University Press.

equator now imposes a high-frequency cutoff. However, one may infer that the waves remain regular only in a flat equatorial channel-type geometry (bottom parallel to surface, both perpendicular to gravity). Since the equation governing the equatorial stream function is again of hyperbolic type, the presence of a slope in the seafloor in zonal direction would enforce again wave focusing and wave attractors but now in the equatorial plane.

6.3. Intermezzo: Controversy Over Laplace's Tidal Equations

[76] In his doctoral thesis, *Solberg* [1928] carried out a theoretical study on internal waves in a neutrally stratified medium, i.e., $N = 0$; as before, we will refer to these waves as "gyroscopic." He included the full Coriolis force, so that the range of allowable frequencies (26) becomes $0 < \omega < 2\Omega$ (for meridional propagation), which includes both the diurnal and semidiurnal tidal frequencies. The theoretical discovery of these gyroscopic tidal waves prompted him and collaborators to conclude that Laplace's tidal equations (LTE) are seriously deficient because they do not admit

wave solutions of this kind [*Bjerknes et al.*, 1933; *Solberg*, 1936]. The point on the deficiency of the LTE was raised independently by *Brillouin and Coulomb* [1933], who examined gyroscopic waves in a rotating cylinder. (The LTE are obtained from (5)–(7) by removing the nonlinear, including metric, terms and making the hydrostatic approximation.) The ensuing debate has been somewhat clouded by confusion, perhaps fueled by a logical weakness in the reasoning put forward by Bjerknes et al. After all, the mere formal existence of gyroscopic waves of tidal frequency does not in itself mean that they must be relevant in the dynamic theory of tides; only if the latter were shown to be the case, could we conclude that LTE are inadequate. It is, furthermore, important to realize that the absence of gyroscopic waves in LTE is primarily due to the hydrostatic approximation, since in a nonhydrostatic setting they do exist irrespective of whether the TA is made (although the TA reduces the latitudinal range for any given frequency, see Figure 11a). Now, *Hylleraas* [1939] brought in a new element in the debate by noticing that *Solberg* [1936] omitted the ocean's vertical density stratification, the inclusion of which, he argued, would render the nontraditional Coriolis terms negligible. This point, while true (provided $N \gg \Omega$), concerns the TA and not the hydrostatic approximation and hence has little bearing on the original issue. But, gradually the debate drifted toward the validity of the TA and the notion that stratification "saves" the LTE. The importance of stratification was reiterated by *Proudman* [1948] and *Miles* [1974]; a comprehensive overview on the assumptions involved in LTE is given by *Hendershott* [1981].

[77] Meanwhile, further insights were obtained in studies ignoring stratification. Thus, for a homogeneous layer of fluid (i.e., $N = 0$), *Longuet-Higgins* [1964] solved LTE and obtained regular solutions of planetary waves in terms of toroidal modes (also called Tesseral harmonics), lacking any variation in radial direction. This solution presents the lowest-order solution in an expansion in relative shell thickness. The incompleteness of these modes was first demonstrated by *Stewartson and Rickard* [1969] upon continuing the expansion in shell thickness in this way removing the TA underlying the LTE. They came to the remarkable conclusion that for subinertial frequencies the next-order fields develop a singularity around the inertial latitude where the characteristics are grazing the inner sphere. The singularity could partly be healed by adding viscosity, but the fine-scale structure remained [*Walton*, 1975]. It thus transpired that the LTE normal mode is, in fact, continuously leaking energy by generating a beam of short-scale gyroscopic waves along the grazing characteristics at the (critical) inertial latitude [*Huthnance*, 1978]. Numerical analysis confirmed the importance of the grazing singularity for the dynamics of a thick homogeneous spherical shell [*Kerswell*, 1995; *Hollerbach and Kerswell*, 1995; *Rieutord and Valdettaro*, 1997; *Fotheringham and Hollerbach*, 1998]. This singularity exists along with wave attractors that were also found. Additionally, quasiperiodic, large-scale wave structures were encountered, familiar from

the gyroscopic wave modes that exist in a full sphere. But, because of their fine structure, most of the physically relevant dissipation was found to take place near the singularities [*Rieutord et al.*, 2001].

7. AN EXCURSION TO ASTROPHYSICAL FLUID DYNAMICS

[78] In this section, we consider stars and giant planets. Although the TA has its roots in geophysical fluid dynamics and is much less commonly used in astrophysical fluid dynamics, there are a few astrophysical subjects wherein it has been adopted, either explicitly or implicitly. These are stellar or planetary (tidal) oscillations and their dissipation (section 7.1) and thermal convection (section 7.2).

7.1. Tidal Oscillations and Dissipation

[79] Surprisingly, the discussion of the influence of rotation on free and (tidally) forced oscillations of stars and giant planets has lagged behind compared to its geophysical counterpart, but, in the last decade, the gap has quickly narrowed. As to the TA, phenomena similar to those discussed above are now also at the astrophysical research front, extending even to general relativistic fluid dynamics of neutron stars [*Maniopoulou and Andersson*, 2004]. Here we discuss the following subjects: first, tidal forcing and dissipation of oscillations in slowly rotating giant planets and stars, where "slowly" means a rotational frequency $\Omega \ll \Omega_{cr}$, where $\Omega_{cr} = (GM/R^3)^{1/2}$ is the Kepler or "breakup" frequency [*Savonije et al.*, 1995; *Savonije and Papaloizou*, 1997; *Ogilvie and Lin*, 2004]; and second, free oscillations of a star [*Dintrans and Rieutord*, 2000]. Both *Savonije et al.* [1995] and *Ogilvie and Lin* [2004] give a comparison of calculations using either the full Coriolis acceleration or the TA. *Savonije and Papaloizou* [1997] and *Dintrans and Rieutord* [2000] do not make the TA at all.

[80] For any star or planet, its radial equilibrium structure is of paramount importance to the structure of its forced and free oscillations. This is particularly true when it comes to the effect of the TA on their qualitative properties or, more specifically, on phenomena such as wave attractors, dispersion relations, and discrete or continuous spectra. Most celestial bodies are built up by concentric shells of different compositional and/or thermodynamic structure. In the present discussion, each shell is considered either solid or fluid. And if fluid, it is either marginally gravitationally unstable in a convective regime ($N = 0$) or stable in a radiative regime ($N^2 > 0$); here N is the buoyancy or Brunt-Väisälä frequency, essentially as defined in (21) (for the precise definition in the astrophysical context, see *Ogilvie and Lin* [2004]). As has already been illustrated in Figure 11, the value of N relative to the rotational frequency Ω determines the qualitative structure of the oscillations, and in a star this may differ from shell to shell.

[81] *Savonije et al.* [1995] and *Savonije and Papaloizou* [1997] discuss tidal forcing by its companion and tidal dissipation of a massive, $20M_\odot$ (i.e., 20 times the mass of the Sun), "zero age main sequence" (ZAMS) star that is

part of a close binary. The radial shell sequence of such a star, as chosen by these authors, is from the center outward: a convective core, an extensive inner radiative envelope, and a shallow outer convective envelope. The core and radiative envelope are about 0.3 and 0.7 of the star's radius R; the outer convective envelope is of very small width but yet of some importance to the problem at hand. In the convective core and envelope, the relevant frequency inequality is $N \sim 0 < 2\Omega$; in the radiative shell, $2\Omega \ll N = O(\Omega_{cr})$. Two regimes of forcing frequencies (in the rotating frame) ω are treated: superrotational ($\omega > 2\Omega$) and subrotational ($\omega \leq 2\Omega$). Although the convective core and envelope support only gyroscopic waves (as before, we will refrain from using the common term "inertial waves") and the radiative shell inertiogravity waves (or, in astrophysical parlance, rotationally modified g modes), the shells cannot be treated separately since both kinds exist at subrotational frequencies. (Compare the overlap in grey regions in Figures 11a and 11d for $\omega < 2\Omega$, implying coupling. Under the TA, by contrast, there is no overlap in the dotted regions in Figures 11a and 11d and hence no coupling.)

[82] Indeed, for forcing in the subrotational regime, *Savonije et al.* [1995] find that there are two dominant effects in the tidal response with respect to applying the TA or not. If the TA is not made, the response for the subrotational frequencies gets swamped by very short wavelength resonances in the convective core and the adjacent regions of the radiative envelope, which in the core reaches amplitudes of several times the equilibrium tide at the star's surface. This singular response is suppressed if the TA is applied. Moreover, if the TA is not made, a subrotational response is found from equator to pole, but applying the TA confines it to regions poleward of the inertial latitude. These conclusions are in line with the properties of gyroscopic and inertiogravity waves as discussed in section 6. Under the TA, $|f|$ serves as an upper bound for gyroscopic waves and as a lower bound for inertiogravity waves; in both cases, the wavelength becomes infinitely long. Without the TA, how-ever, waves always become short at their lower and upper bounds, as is evident from (32). Furthermore, the confinement of subrotational response to regions poleward of the inertial latitude is a feature of the TA if $N = 0$ (see Figure 11a). This confinement is thus an artifact of the TA, as is the suppression of short-wavelength low-frequency oscillations.

[83] It is now interesting to compare these results on tidally forced oscillations to those of *Dintrans and Rieutord* [2000] on free oscillations. Their setting is a lower-mass ZAMS star (γ Doradus type) of 1.5 $M_\odot$, with a radial structure like above, except that the outer (convective) envelope is now thicker. They start with some important remarks concerning the mathematical problems entailed in the calculation of eigenmodes and eigenfrequencies of rotating stars. First, the usual practice in astrophysics of calculating the eigenfrequencies by expanding them in a power series in the rotation rate Ω around their values of the nonrotating state is only valid for very slow rotation and will not converge for strong rotation. Second, the alternative of trying to calculate the eigenfrequencies directly from the
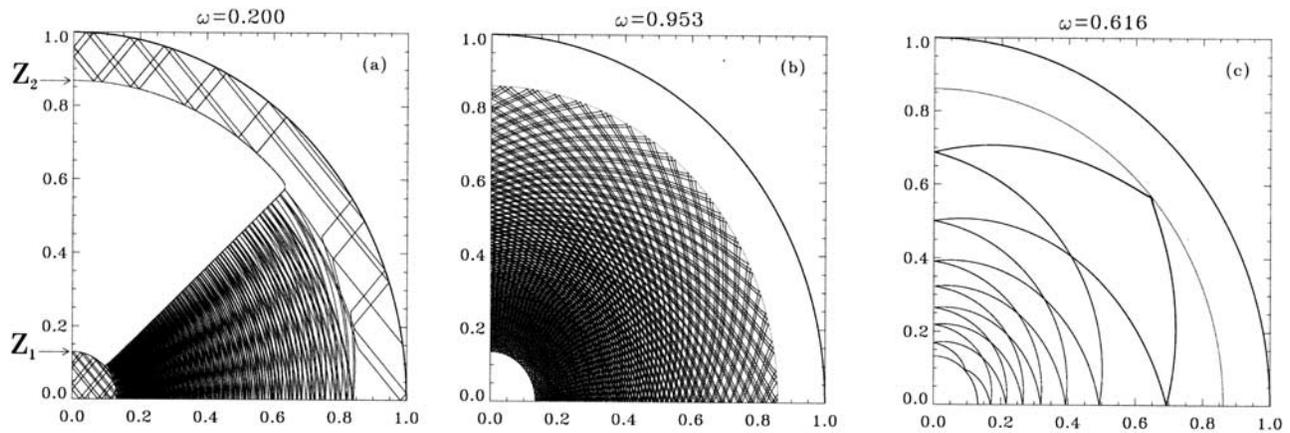
Figure 23. Webs of characteristics in a star for (a) a subrotational frequency ($\omega < 2\Omega$) and (b and c) superrotational ones ($\omega > 2\Omega$). The inner and outer layers are convective ($N = 0$); the middle layer is radiative ($N \gg 2\Omega$); the transition between the spherical layers is indicated by Z_1 and Z_2. These results were obtained by including the full Coriolis force. (If the TA were made, the gyroscopic waves in the inner and outer shells in Figure 23a would exist only at high latitudes, in which case the coupling with the middle layer would be destroyed.) From *Dintrans and Rieutord* [2000]. Reprinted with permission.

equations of motion in a rotating frame leads to an infinite series of coupled equations because of rotational mode coupling, the truncation of which does not guarantee a convergent result either, particularly for low-frequency inertiogravity waves of high radial order for which $\omega \sim$ $<2\Omega$. They then refer to their fundamental results for a single reflective rotating shell [*Rieutord and Valdettaro*, 1997; *Dintrans et al.*, 1999] and conclude that the mixed hyperbolic/elliptic operator that describes internal inertiogravity wave propagation in a rotating shell gives rise to wave focusing and the phenomenon of wave attractors. Since attractors, indeed, require the sum of an infinite number of spherical harmonics to reproduce them, the usual ordering of eigenvalues in the degree of the harmonic and the radial order no longer makes sense. The conclusion then is that a nonperturbative approach is necessary for resolving these orbits. It should be noted that this requires from the outset a nontraditional approach since no attractors are possible in this case when the TA is used; under the TA, the internal wave solutions are regular, their radial and meridional structures being separable (the latter contains Airy turning points); see the discussion by *Miles* [1974].

[84] As the star considered by *Dintrans and Rieutord* [2000] has no solid core, any wave attractor that might occur must find its origin in the reflective properties of the interfaces of the different shells and the outer boundary, the latter being treated under the rigid lid approximation. First, it is shown that a nonrotating star contains the familiar pure gravity waves trapped within the radiative envelope; here the turning surfaces are spheres. Introducing rotation makes these surfaces complicated in that they become nonspherical, crossing the spherical shells, and thus the wave operator also becomes mixed in the meridional direction. This can lead to additional trapping in the meridional plane, depending on the value of stratification N and the wave frequency. For the classification of possible wave modes, the scheme of *Friedlander and Siegmann* [1982] and

Dintrans et al. [1999] is used, as discussed in the beginning of section 6. At subrotational frequencies, gyroscopic waves exist throughout the convective layers (as H_1 modes), while in the radiative layer, inertiogravity waves are trapped equatorward of their critical latitude (H_2 modes); the two are coupled. See Figure 23a. (As discussed in section 6.1.3, TA would destroy the coupling.) Characteristics are straight lines for gyroscopic modes in the neutrally stratified regime of the inner core and outer shell and are nearly circles for inertiogravity waves in the strongly stratified central shell. At superrotational frequencies, on the other hand, only inertiogravity waves exist in the radiative core (as E_1 modes); see Figures 23b and 23c.

[85] Characteristic orbits can also be divided in "ergodic" ones, filling the whole hyperbolic domain (Figure 23b), as they always are in the stably stratified nonrotating case, or "periodic" ones (Figure 23c). The latter are wave attractors on which all characteristics of a finite continuous band of frequencies focus. Although in the present case most of these bands have small width and thus most frequencies possess an ergodic characteristic, the number of bands connected to an attractor increases with rotation rate, and they then crowd increasingly at the subrotational side of the spectrum.

[86] We now return to the problem of tidally forced oscillations and their dissipation as discussed by *Ogilvie and Lin* [2004]. Their prototype is the planet Jupiter and its tides as forced by its companion Io. For Jupiter, the radial shell sequence used by these authors is a solid core, an extensive convective envelope, and a radiative outer envelope in the fractions 0.1, 0.7, and 0.2, respectively, of the planet's radius (see section 7.2 for further remarks on Jupiter's interior structure). Such a sequence can also stand for exoplanets and low-mass ZAMS stars. *Ogilvie and Lin* [2004] provide an extensive comparison between tidal excitation with and without the TA (and also without any Coriolis effects at all). In an earlier study, *Ioannou and*
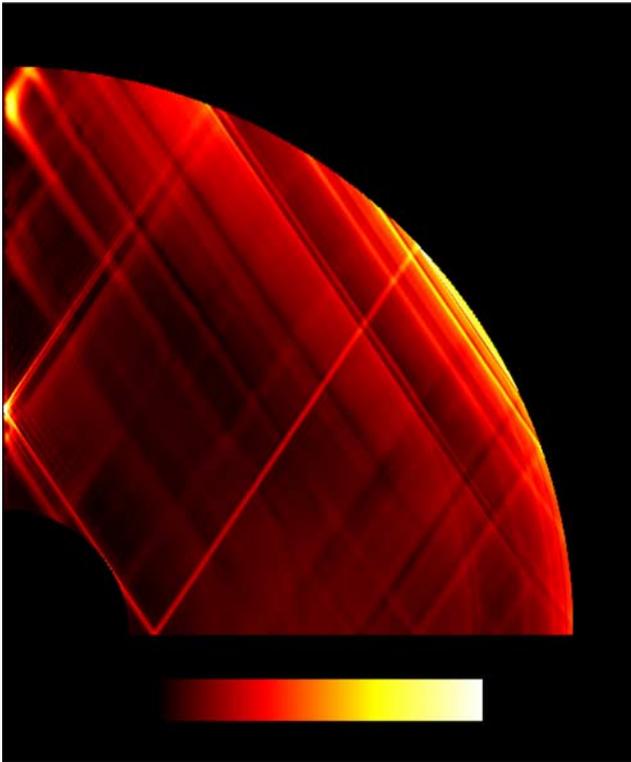
Figure 24. High-resolution calculation showing the pattern of the tidal response of a uniformly rotating planet. The RMS velocity of the total tide (equilibrium plus dynamic) is plotted in a meridional slice through the convective region only. The velocity scale is linear, black representing zero. The forcing frequency is chosen to be near the peak of a gyroscopic-mode resonance. From *Ogilvie and Lin* [2004]. Reproduced by permission of the AAS.

Lindzen [1993a, 1993b] had already found that the TA could describe the tides in the radiative shell reasonably well, while it was not appropriate in the adiabatic interior of Jupiter, the gyroscopic waves of which, however, they did not consider relevant to the tidal dissipation problem. But, *Ogilvie and Lin* [2004] note that the tidal forcing frequency is in the subrotational range, so that gyroscopic waves are, in fact, likely to be excited in the convective shell. By including a small amount of viscosity, *Ogilvie and Lin* [2004] numerically computed the tidal dissipation rate in the convective shell (split up into that due to viscosity within the convective shell and to gyroscopic waves leaking away into the radiative shell as inertiogravity waves). Resonances show up as maxima in the dissipation rate. Using the full Coriolis force, they find that in the subrotational frequency range strong resonances appear, which become increasingly dense and of strongly irregular amplitude distribution if viscosity is lowered, so that "a resonant response is almost guaranteed for any forcing frequency in the subrotational range," the spectrum becoming dense or continuous. Furthermore, the dissipation rate does not seem to vanish for vanishing viscosity. The resonance peaks in the subrotational regime are connected to wave attractors on which the viscous dissipation is concentrated because of the

very strong shear at the attractor. The most prominent attractor is the one that emanates from the critical latitude at the core boundary. An example of the spatial structure of a characteristic web with an attractor is shown in Figure 24.

[87] By contrast, using the TA gives a completely distorted response spectrum with a dense set of subrotational resonances superposed on broad global resonance "shoulders" on both sides of the zero frequency. These "shoulders" are clearly an artifact of the TA, probably due to decoupling of radial and angular motion, giving a strong global subrotational response. As already discussed above, wave attractors in the subrotational regime of the convective core are not expected to occur with the TA. Finally, the TA overestimates the viscous tidal dissipation rate by 2 orders of magnitude and should therefore according to *Ogilvie and Lin* [2004, p. 498], "never be used for inertial [i.e., gyroscopic] waves in gaseous giant planets." It seems appropriate to extend this conclusion to any celestial body that carries a substantial convective shell.

7.2.   Thermal Convection on or in a Rotating Planet

[88] The celestial bodies of section 7.1, rotating gas giant planets and stars, usually have extensive convective shells in their interior produced by internal heating (and sometimes by chemical fractionation). Without rotation, this convection would be of the Rayleigh-Bénard type with an overall spherical symmetric pattern of convective rolls that transport the internally generated heat outward. Under strong rotation, this picture changes drastically. Rotation breaks the spherical symmetry in the sense that convective rolls tend to align with the rotation axis forming Taylor-Proudman columns [*Taylor*, 1923]. *Veronis* [1959] has shown that on a rotating plane the Taylor-Proudman constraint leads to columnar cells in which the convective flow spirals upward and downward, as illustrated in Figure 25 [see also *Chandrasekhar*, 1961]. This is reminiscent of the deep convection in the polar oceans as discussed in section 4. *Busse* [1976] proposed that in the spherical setting of a rotating convective planet, the alignment of the convection cells with the rotation axis leads to rolls perpendicular to the equatorial plane in the planet's interior (Figure 26). This is reminiscent of the deep-equatorial jets of section 5.3. It thus appears that the thin shells of the Earth's atmosphere and ocean and the deep convection of giant planets have characteristics in common, a theme that has been elaborated upon by *Colin de Verdière and Schopp* [1994] and *Schopp and Colin de Verdière* [1997]. We shall now discuss recent progress in understanding convection of a giant planet, Jupiter, where the question of TA or non-TA shows up in a disguised form in the question of "thin shell" or "deep shell." (The results also apply to Saturn but not to Neptune or Uranus, which have a different internal structure.) In this, we shall follow the excellent recent review of Jovian dynamics by *Vasavada and Showman* [2005] to which we refer the reader for a much more detailed discussion than can be presented here.

[89] Jupiter's interior consists of a small solid core, an extensive hydrogen shell that can be divided into a molec-
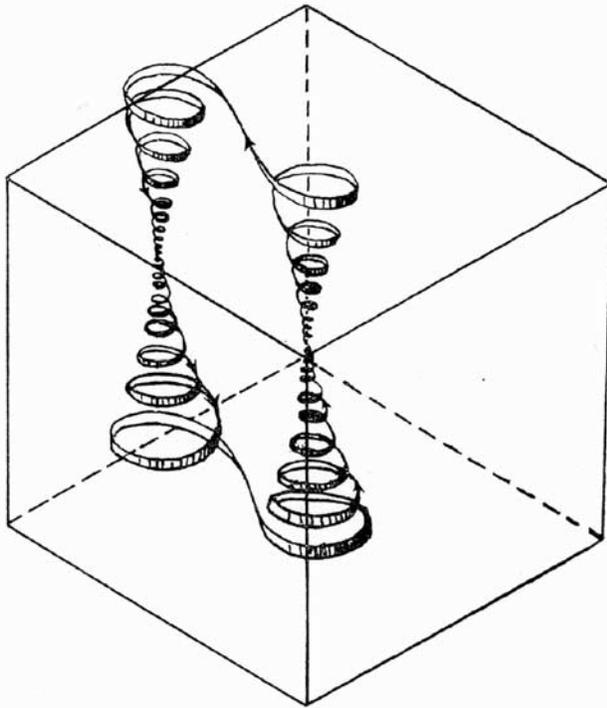
Figure 25. Columnar rotating convection cells. The gravitational acceleration and the rotation vector are both perpendicular to the bottom plane. From *Veronis* [1959].

ular outer and a metallic inner region, and a shallow troposphere [*Guillot*, 2005]. It is thought that convection is restricted either to the molecular layer of uncertain depth (deep convection) or to the troposphere only (shallow convection) and that the transition from the molecular to the metallic shell is diffuse and thus not well defined. All that is visible of Jupiter's interior activity from the outside occurs in the shallow troposphere on top of the molecular hydrogen shell. The troposphere contains Jupiter's characteristic cloud bands (Figure 27). This banded structure is the reflection of a system of approximately 30 zonal jets from pole to pole with a doubly peaked strong prograde jet at the equator (Figure 28a). Every theory of convection must ultimately explain the zonal jet structure in all its detail (the prograde equatorial jet, its amplitude and width, and the number, width, and amplitude of the smaller jets at higher latitudes). Broadly speaking, there are two sorts of theory that have been developed for explaining the jet structure as a result of convection. The reason for including these in this review is that the two lines of approach can be seen as implicitly TA and explicitly non-TA.

[90] In the thin shell approach, convection is thought to be restricted to the outer layer, the troposphere, and to lead to a turbulent state. Because of the planet's rotation and possibly a static vertical stability produced by latent heat release in the cloud bands, the turbulence is quasi-two-dimensional. In its simplest form, the turbulence can then be described by the 2-D shallow water equations or their derivate, the quasigeostrophic vorticity equation on a sphere

(either including 2-D divergent flow or not), both of which imply the TA. Apart from making the "thin shell" and the "shallow water" approximation, for later reference it is important to stress two more properties of such an approach: the 2-D shallow water or the vorticity equations on a sphere are based on the non-Euclidean metric of the spherical surface [*Müller*, 1992], and fluid columns are implicitly thought to move with their axes always in the vertical direction, defined by the local gradient of the effective gravity potential. This also applies to Taylor columns, and the Taylor-Proudman constraint thus necessarily weakens in the equatorial direction as a result of the TA. Their "TA character" is implicit in the sense that fluid columns move in an artificial planetary vorticity gradient in the meridional direction and conserve their absolute vorticity by an artificial "Coriolis torque" on the fluid column when moving in that gradient ("artificial" here means due to making the TA). If we now choose the 2-D nondivergent vorticity equation as the simplest way to describe the evolution of 2-D turbulence, then in a planar setting, rotating or not, this kind of turbulence has the property of transferring energy from the injection (forcing) scale to ever larger scales by vortex merging until the domain size is reached. However, in the shallow water approximation under the TA, a rotating spherical shell is an anisotropic medium that carries Rossby waves with an anisotropic dispersion relation. When vortex merging then leads to length scales comparable to the Rossby wave length or, equivalently, when the advection timescale L/U of a vortex of length L and characteristic velocity U matches the Rossby wave period, vortex merging breaks down, and wave dynamics takes over [*Rhines*, 1975]. The dispersion
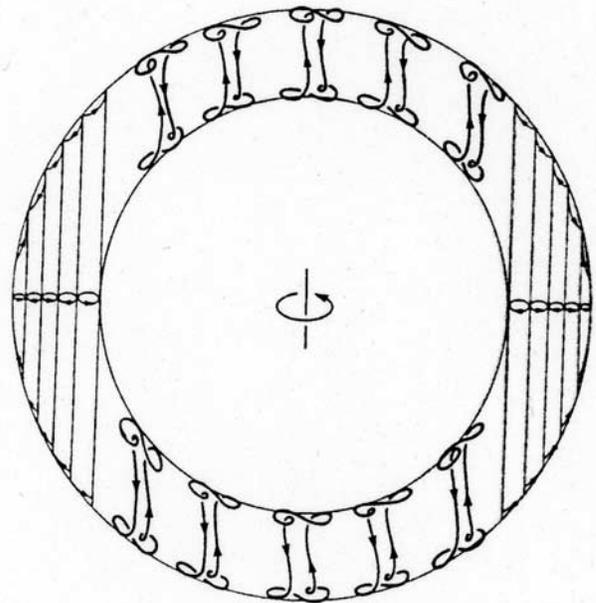
Figure 26. Columnar convection in equatorial and polar regions of a giant planet like Jupiter. From *Busse* [1994]. Reused with permission: copyright 1994, American Institute of Physics.

Figure 27. True-color mosaic of Jupiter acquired by Cassini. The portrait shows Jupiter's zonal bands, the Great Red Spot and other vortices, several discrete storms within the orange band north of the equator and also west of the Great Red Spot, and two equatorial hot spots at the northern edge of the equatorial band near the planetary limb. NASA image PIA04866. PIA images can be accessed at NASA's Planetary Photojournal, http://photojournal.jpl.nasa.gov.

relation of a (nondivergent) Rossby wave in its local form (the beta plane) reads as follows:

$$\omega = -\frac{\beta k_x}{k_x^2 + k_y^2} = -\frac{\beta \cos \theta}{|k|},$$

where ω is the frequency, k_x and k_y are the longitudinal and latitudinal wave numbers, and θ is the angle of Rossby wave propagation with respect to the positive x axis (i.e., eastern direction). This relation traces, for a given frequency, a circle in the $k_x k_y$ plane with its center at $(x = -\beta/2\omega, y = 0)$ and radius $\beta/2\omega$. The smallest accessible wave numbers for the energy cascade when the advection timescale reaches the Rossby wave period are now located near the origin of the $k_x k_y$ plane, where the wave number vector is smallest and nearly meridional, whence the wave crests are nearly zonally oriented. The characteristic meridional width of these zonally elongated eddies is then given by the so-called Rhines scale $L_\beta = (U/\beta)^{1/2}$. Finally, zonal jets appear as a rectified flow generated by these strongly anisotropic eddies.

[91] This interesting explanation of the zonal jets succeeds rather well in explaining the zonal jet structure in the midlatitudes and high latitudes of Jupiter. It, however, fails at the equator where it predicts a retrograde jet instead of a prograde one. This failure is a consequence of mixing of vorticity (or, for that matter, of angular momentum) by 2-D turbulence in a thin shell over a region around the equator, which reduces the angular momentum at the equator, reflected in the retrograde jet [*Yano et al.*, 2005] on the assumption of a dissipative medium without which the nonacceleration theorem holds and no rectified flow is possible.
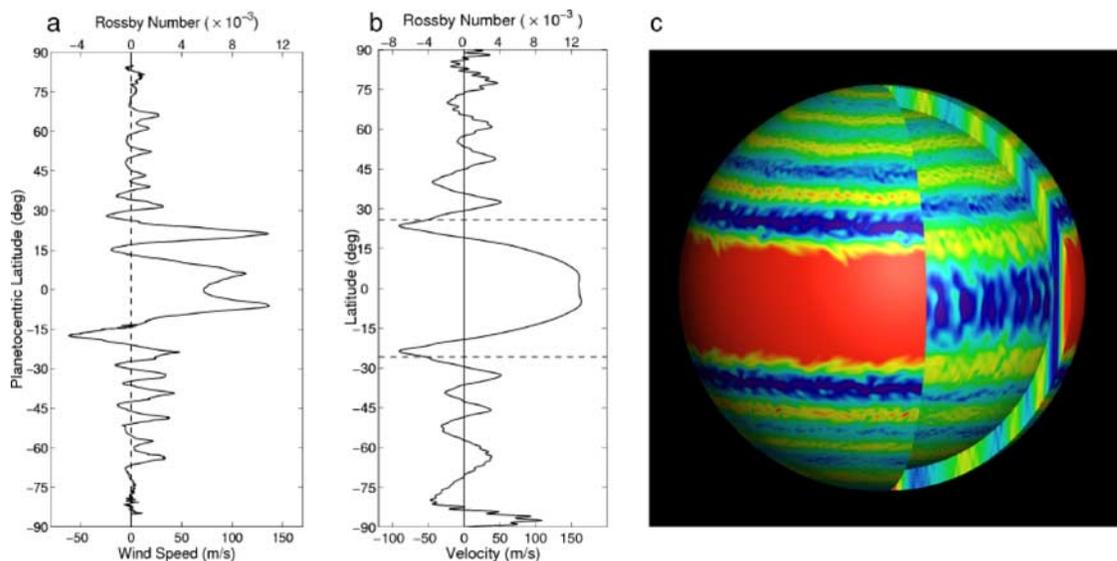
Figure 28. (a) Observed zonal wind pattern of Jupiter. (b) Simulated zonal wind pattern. (c) Snapshot of the simulated azimuthal velocity field on the inner and outer spherical surface and on a meridional slice. Red is prograde flow, and blue is retrograde flow. Reprinted by permission from Macmillan Publishers Ltd: *Nature* [*Heimpel et al.*, 2005], copyright 2005, http://www.nature.com/nature/index.html.
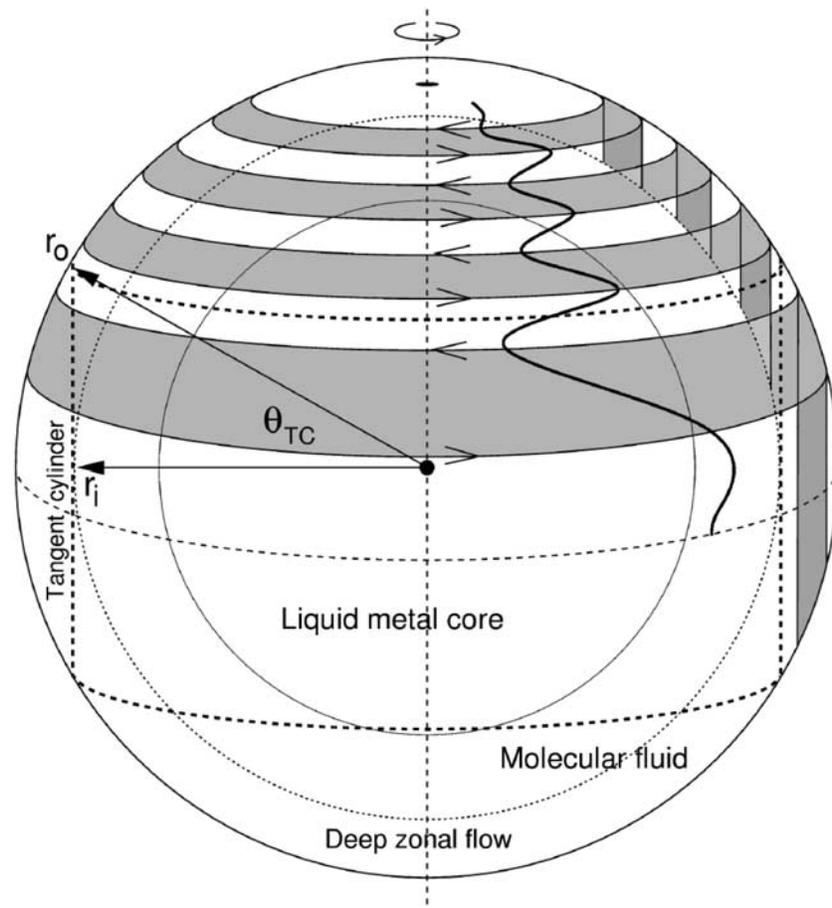
Figure 29. Illustration of the shell structure and the location of the tangent cylinder. Reprinted by permission from Macmillan Publishers Ltd: *Nature* [*Heimpel et al.*, 2005], copyright 2005, http://www.nature.com/nature/index.html.

[92] We now turn to the other extreme: deep convection. As has already been noticed, it is not well known how deep the convective layer of Jupiter really is. If we first suppose that the whole of the interior is in a convective state, which is certainly not so, then a remarkable similarity exists in the dynamics of deep turbulent convection in a sphere with that of shallow water turbulence on a sphere. In the sphere, according to the Taylor-Proudman theorem all convection is thought to be columnar with the roll axes in the direction of the rotation axis. This setting is thus principally non-TA, and the description of its dynamics is best done in a cylindrical coordinate system (see also section 5.2). Moreover, the metric of the space in which the columns are restricted to move, i.e., the equatorial plane, is a Euclidean space in contrast to that of the shallow water equations on a sphere. The position of a column is given by a radial and an azimuthal coordinate only, and its height is determined by the radial coordinate because of the spherical surface, rigid by assumption, surrounding the fluid. The latter is the clue to the similarity noticed above as it introduces an anisotropy in the sense that if columns move radially, they are stretched or compressed, and if they move azimuthally, they are not. If they conserve potential vorticity, they will spin up or down when moving radially. In other words, the medium carries so-called "thermal Rossby waves" [*Busse*, 1994,

2002] with the topographic beta effect of the spherical surface as the restoring mechanism. But, there is an important difference with the shallow water approach in a thin shell: the planetary potential vorticity gradient, the topographic beta term so to speak, has opposite sign as the columnar height decreases in the outward direction [*Ingersoll and Pollard*, 1982]. This immediately implies that potential vorticity mixing in the outer layers produces a prograde jet in the equatorial region. Outside the equatorial region, however, this approach fails to produce zonal jets of sufficient number and strength, apparently because of the strong decrease of the beta effect poleward.

[93] The outcome of the former two paragraphs seems to be that a successful theory of explaining the Jovian zonal bands as a result of convection should use "the best of two worlds." Indeed, recently, simulations of Jupiter's (and Saturn's) zonal jet structure by a hybrid model of potential vorticity dynamics have succeeded in reproducing the required prograde equatorial jet together with a realistic midlatitudinal and higher-latitudinal structure of zonal jets [*Heimpel et al.*, 2005; *Heimpel and Aurnou*, 2007]. If it is supposed that the convective layer is moderately deep, i.e., extends from the surface to about 0.9 of Jupiter's radius, which is only a fraction of the molecular hydrogen layer, then the inner structure of the convection in such a shell can

be subdivided into two sections separated by the "tangent cylinder" touching the inner boundary of the convecting shell (Figure 29). Outside the tangent cylinder, the convection is of the "deep" sort; that is, columns are able to move in the equatorial plane between the outer and inner concentric boundaries of the shell. This produces the equatorial prograde jet as the potential vorticity gradient is inwardly directed (Figures 28b and 28c). Inside the cylinder, however, the same gradient is outwardly directed; that is, it has the same sign as the beta term in the 2-D vorticity equation of the shallow water approximation and thus produces zonal jets in the shell in much the same way as on the sphere in the shallow water approach (Figures 28b and 28c). However, its dynamics is different from the shallow water approach and from the dynamics in the outer region in the following aspects: (1) The columns move in the radial, azimuthal and vertical (i.e., rotational) direction keeping the column axis always aligned to the rotation axis, in contrast to columns in the "thin" shell approximation using the shallow water equations under the implicit TA; their vertical coordinate is therefore not free but set by the radial coordinate (or vice versa). (2) In doing so, they move in a non-Euclidean 2-D space along a spherical surface, as in the "thin" shell, in contrast to the columns in the region outside the cylinder. (3) As Taylor columns, keeping their axis always aligned to the rotation axis, their dynamics is definitely non-TA, like it is for the columns in the region outside the tangent cylinder. The tangent cylinder is thus in several senses a singular boundary: it divides the outer region with cross-equatorial columns from two separate polar inner regions each with a potential vorticity gradient opposite to that of the outer region and each with a metric different from the outer region.

[94] All in all, and this is, of course, the principal reason for discussing rotating convection on and in a sphere in this review, a strictly non-TA approach appears to be preferred in explaining the zonal jet structure of Jupiter and Saturn.

8. CONCLUSION AND PERSPECTIVES

[95] A quarter century ago, *Hendershott* [1981, p. 297] concluded with regard to the TA: "its domain of validity has not yet been entirely delineated." This is still true today, but, as the preceding sections show, it has since become much clearer what phenomena are likely to be affected by the TA. A common thread between various topics discussed here is the occurrence of a tilt, which is due to the fact that the rotation axis is no longer aligned to gravity if one abandons the TA. The most extreme example is found in the idealized concept of Taylor columns near the equator, whose axes are aligned to the rotation axis and thus are oriented horizontally (section 5.2); a similar phenomenon occurs in patterns of thermal convection in giant planets (section 7.2). Numerical models show that convective plumes at higher latitudes equally undergo a tilt toward the rotation axis; meddies are weakly tilted (section 4). Finally, the asymmetry in internal wave propagation can

also be traced back to a realignment, as is most clearly seen in gyroscopic waves (Figure 13).

[96] Some studies fall outside the main categories discussed so far. For example, *Backus* [1962] examined the role of nontraditional terms in surface inertiogravity waves, and a new obliquely rotating set of "shallow water equations" (but with first-order nonhydrostatic and nontraditional effects included) was formulated by *Dellar and Salmon* [2005]. The dispersion relation showed that short inertiogravity waves are the most affected, but the departure from traditional theory is not dramatic; from these studies, one can safely conclude that nontraditional effects may be neglected here.

[97] As demonstrated in section 6, the situation is very different for internal waves. Scaling arguments have sometimes been used to show that the effect of $\tilde{f}$ becomes negligible for strong stratification in the sense that $N \gg 2\Omega$, but this condition is satisfied only within the thermocline. Moreover, while it is true that the role of $\tilde{f}$ is most prominent in weakly stratified layers, scaling arguments cannot be entirely trusted because the TA has the character of a singular limit. The subinertial short-wave limit, which exists no matter how strong the stratification is but disappears under the TA, is a case in point (section 6.1.2). These short subinertial waves are trapped in weakly stratified layers and may play some role in ocean dynamics in a wider sense (e.g., deep-ocean mixing), but this has yet to be explored.

[98] One elementary but far-reaching consequence of abandoning the TA is the enlargement of the range of allowable internal wave frequencies. The starkest contrast with the TA occurs if one has adjacent layers of very weak ($N \approx 0 \ll 2\Omega$) and stronger ($N > 2\Omega$) stratification, the former being typically the case in convective layers. The frequency ranges for the two layers are then disjoint under the TA; in other words, internal waves of a certain frequency that exist in one layer are excluded from the other layer. If one abandons the TA, however, an overlap between the ranges is found, allowing (near-inertial) waves to pass from one layer into the other. Observational evidence supports this (section 6.1.3). An example of such an overlap in the astrophysical context is shown in Figure 23a. The role of $\tilde{f}$ gains further importance in that it acts as a symmetry breaker, which, in turn, is a necessary condition for the occurrence of internal wave attractors (section 6.2.2); these attractors affect tidal dissipation in giant planets and stars (section 7.1).

[99] Although the larger part of the "nontraditional" literature has dealt with internal waves, in recent years various kinds of mesoscale phenomena have attracted much attention as well. The studies discussed in section 3.2 suggest that Ekman dynamics is significantly affected by $\tilde{f}$, especially in that it introduces horizontal anisotropy and hence a fundamental dependence on wind direction, but we should add the cautionary note that all these studies have neglected stratification. This lacuna needs to be filled to establish what, realistically, the effects of $\tilde{f}$ could be in the ocean.

[100] The dynamics near the equator is of extraordinary complexity, and a unified picture is still lacking; the detailed observations on equatorial flows made in recent years (some of it mentioned in this review) still often lack proper theoretical interpretation. Yet the literature discussed here suggests that $\tilde{f}$ is likely to play a role in a satisfactory explanation of the observed phenomena. Its importance is furthermore seen in the nontraditional thermal wind balance; see equations (15) and (16).

[101] *Sheremet* [2004] demonstrated that examining nontraditional effects is feasible even in laboratory experiments. An encouraging conclusion that transpires from this review is that there is often no need to make the TA in analytical studies; the basic theory of internal waves, for example, is as simple without as with the TA. For all the topics discussed in this review, observational work dedicated to examining nontraditional effects is still scarce but would provide a much needed test for the theories and models that have been developed. In numerical studies, the inclusion of the nontraditional terms poses no hurdle at all and can be consistently done in a nonhydrostatic or quasi-hydrostatic setting [*Marshall et al.*, 1997]. Indeed, as *White and Bromley* [1995] note, since the early 1990s the full Coriolis force has been incorporated in the weather prediction model of the U.K. Met Office; this suggests it might some day become traditional not to make the traditional approximation!

APPENDIX A: DERIVATION OF CORIOLIS COMPONENTS

[102] The four components of the Coriolis force, as stated in Table 1, can all be derived from elementary mechanical principles. For the benefit of the general reader, we outline the derivation below. We notice that in an arbitrarily oriented coordinate system, as employed by *Coriolis* [1835], one finds six Coriolis terms in total; however, if one adopts the usual geographical system, as did Laplace, four terms appear instead of six because the rotation vector is then perpendicular to one of the coordinates' basic vectors (namely, the zonal one).

[103] From the terrestrial perspective, a fluid parcel at rest on the Earth is subject to a balance of forces. From the perspective of the "fixed stars," the parcel traverses a latitudinal circle of radius $R_\phi = R\cos\phi$ at an eastward velocity $U = \Omega R_\phi$. The centripetal force (U^2/R_ϕ) required for this circular motion is provided by gravity and pressure gradients. We now consider three cases in which the parcel, instead of being at rest, has a velocity of its own. (1) If the parcel has an eastward velocity u, its total velocity will be $U+u$, enhancing the required centripetal force by an amount $2Uu/R_\phi$ (to first order, assuming $u \ll U$), or, using the definition of U, $2\Omega u$. From the terrestrial perspective, this increment acts as a centrifugal force, tending to sweep the parcel outward in the latitudinal plane. This outward acceleration can be decomposed into a radial component $2\Omega u\cos\phi = \tilde{f}u$ and a southward one, $-2\Omega u\sin\phi = -fu$, in

the Northern Hemisphere (northward in the SH). This is precisely the result stated in the first row of Table 1. (2) If in the NH the parcel moves northward to latitude $\phi' = \phi + \delta\phi$, its latitudinal circle becomes smaller by an amount $-R\sin\phi\ \delta\phi$ (to first order). By conservation of angular momentum ($UR_\phi = (U + u)R_{\phi'}$), it will obtain an eastward velocity of its own: $u = \Omega\sin\phi\ R\delta\phi$. Parcels at rest at latitude ϕ', meanwhile, rotate at $U' = \Omega R_{\phi'} \approx U - \Omega\sin\phi\ R\delta\phi$. With respect to those parcels, the initially northward moving parcel will thus get an excess of eastward velocity of $2\Omega\sin\phi\ R\delta\phi = fR\delta\phi$, equivalent to an eastward acceleration fv, as stated in the second row of Table 1. (3) Finally, we consider a parcel that moves initially upward (i.e., radially outward) to $R' = R + \delta R$. Again from the perspective of the "fixed stars" and by conservation of angular momentum ($UR_\phi = (U + u)R'_\phi$), the parcel will get a smaller eastward velocity by an amount $u = -\Omega\cos\phi\ \delta R$. Ambient parcels at rest at this higher altitude have an eastward velocity $U' = \Omega R'_\phi$, an excess compared to U, i.e., of $\Omega\cos\phi\ \delta R$. With respect to those parcels, the initially upward moving parcel will thus get an excess of westward velocity of $-2\Omega\cos\phi\ \delta R = -\tilde{f}\delta R$, equivalent to a westward acceleration $-\tilde{f}w$, as stated in the third row of Table 1.

[105] The Editor responsible for this paper was Henk Dijkstra. He thanks three technical reviewers and one anonymous cross-disciplinary reviewer.

REFERENCES

Backus, G. E. (1962), The effect of the Earth's rotation on the propagation of ocean waves over long distances, *Deep Sea Res. Oceanogr. Abstr.*, 9, 185–197.

Badulin, S. I., V. M. Vasilenko, and M. I. Yaremchuk (1991), Interpretation of quasi-inertial motions using Megapoligon data as an example, *Izv. Atmos. Ocean. Phys.*, 27(6), 446–452.

Baines, P. G., and J. W. Miles (2000), On topographic coupling of surface and internal tides, *Deep Sea Res., Part I*, 47, 2395–2403.

Beckmann, A., and S. Diebels (1994), Effects of the horizontal component of the Earth's rotation on wave-propagation on an *f*-plane, *Geophys. Astrophys. Fluid Dyn.*, 76, 95–119.

Bjerknes, V., J. Bjerknes, H. Solberg, and T. Bergeron (1933), *Physikalische Hydrodynamik*, 797 pp., Springer, Berlin.

Bourlès, B., et al. (2003), The deep currents in the eastern equatorial Atlantic Ocean, *Geophys. Res. Lett.*, 30(5), 8002, doi:10.1029/2002GL015095.

Brekhovskikh, L. M., and V. Goncharov (1994), *Mechanics of Continua and Wave Dynamics*, 342 pp., Springer, Berlin.

Bretherton, F. P. (1964), Low frequency oscillations trapped near the equator, *Tellus*, 16, 181–185.

Brillouin, M., and J. Coulomb (1933), *Oscillations d'un liquide pesant dans un bassin cylindrique en rotation*, 70 pp., Gauthier-Villars, Paris.

Burstyn, H. L. (1966), Early explanations of the role of the Earth's rotation in the circulation of the atmosphere and the ocean, *Isis*, 57(2), 167–187.

Busse, F. H. (1976), A simple model of convection in the Jovian atmosphere, *Icarus*, 29, 255–260.

Busse, F. H. (1994), Convection driven zonal flows and vortices in the major planets, *Chaos*, *4*, 123–134.

Busse, F. H. (2002), Convective flows in rapidly rotating spheres and their dynamo action, *Phys. Fluids*, *14*, 1301–1314.

Chandrasekhar, S. (1961), *Hydrodynamic and Hydromagnetic Stability*, 652 pp., Oxford Univ. Press, Oxford, UK.

Coleman, G. N., J. H. Ferziger, and P. R. Spalart (1990), A numerical study of the turbulent Ekman layer, *J. Fluid Mech.*, *213*, 313–348.

Colin de Verdière, A. (2002), Un fluide lent entre deux sphères en rotation rapide: Les théories de la circulation océanique, *Ann. Math. Blaise Pascal*, *9*(2), 245–268.

Colin de Verdière, A., and R. Schopp (1994), Flows in a rotating spherical shell: The equatorial case, *J. Fluid Mech.*, *276*, 233–260.

Coriolis, G. (1835), Mémoire sur les équations du mouvement relatif des systèmes de corps, *J. Éc. Polytech. Paris*, *XXIV*(XV), 142–154.

Dellar, P. J., and R. Salmon (2005), Shallow water equations with a complete Coriolis force and topography, *Phys. Fluids*, *17*(10), 106601, doi:10.1063/1.2116747.

Denbo, D. W., and E. D. Skyllingstad (1996), An ocean large-eddy simulation model with application to deep convection in the Labrador Sea, *J. Geophys. Res.*, *101*(C1), 1095–1110.

Dengler, M., and D. Quadfasel (2002), Equatorial deep jets and abyssal mixing in the Indian Ocean, *J. Phys. Oceanogr.*, *32*, 1165–1180.

Dintrans, B., and M. Rieutord (2000), Oscillations of a rotating star: A non-perturbative theory, *Astron. Astrophys.*, *354*, 86–98.

Dintrans, B., M. Rieutord, and L. Valdettaro (1999), Gravito-inertial waves in a rotating stratified sphere or spherical shell, *J. Fluid Mech.*, *398*, 271–297.

d'Orgeville, M., B. L. Hua, and H. Sasaki (2007), Equatorial deep jets triggered by a large vertical scale variability within the western boundary layer, *J. Mar. Res.*, *65*, 1–25.

Dubois, E. (1885), Résumé analytique de la théorie des marées telle qu'elle est établie dans la Mécanique Céleste de Laplace, *Rev. Marit. Colon.*, *85*, 116–154, 419–460, 687–710.

Durran, D. R., and C. Bretherton (2004), Comments on "The roles of the horizontal component of the Earth's angular velocity in nonhydrostatic linear models," *J. Atmos. Sci.*, *61*, 1982–1986.

Eckart, C. (1960), *Hydrodynamics of Oceans and Atmospheres*, 290 pp., Pergamon, New York.

Ekman, V. W. (1905), On the influence of the Earth's rotation on ocean currents, *Ark. Mat. Astron. Fys.*, *2*(11), 1–52.

Ekman, V. W. (1932), Studien zur Dynamik der Meeresströmungen, *Gerlands Beitr. Geophys.*, *36*, 385–438.

Emanuel, K. A. (1979), Inertial instability and mesoscale convective systems. part I: Linear theory of inertial instability in rotating viscous fluids, *J. Atmos. Sci.*, *36*, 2425–2449.

Etling, D. (1971), Einfluß der thermischen Schichtung auf der Stabilität einer Ekman'schen Grenzschichtströmung, *Beitr. Phys. Atmos.*, *44*, 168–186.

Firing, E. (1987), Deep zonal currents in the central equatorial Pacific, *J. Mar. Res.*, *45*, 791–812.

Fotheringham, P., and R. Hollerbach (1998), Inertial oscillations in a spherical shell, *Geophys. Astrophys. Fluid Dyn.*, *89*, 23–43.

Friedlander, S., and W. L. Siegmann (1982), Internal waves in a rotating stratified fluid in an arbitrary gravitational field, *Geophys. Astrophys. Fluid Dyn.*, *19*, 267–291.

Fritts, D. C., and M. J. Alexander (2003), Gravity wave dynamics and effects in the middle atmosphere, *Rev. Geophys.*, *41*(1), 1003, doi:10.1029/2001RG000106.

Fruman, M. D. (2005), Equatorial symmetric instability, 178 pp., Ph.D. thesis, Univ. of Toronto, Toronto, Ont., Canada.

Galperin, B., A. Rosati, L. H. Kantha, and G. L. Mellor (1989), Modeling rotating stratified turbulent flows with application to oceanic mixed layers, *J. Phys. Oceanogr.*, *19*, 901–916.

Garrett, C., and L. St. Laurent (2002), Aspects of deep ocean mixing, *J. Oceanogr.*, *58*, 11–24.

Garwood, R. W. (1991), Enhancements to deep turbulent entrainment, in *Deep Convection and Deep Water Formation in the Oceans*, edited by P. C. Chu and J. C. Gascard, pp. 197–213, Elsevier, Amsterdam.

Garwood, R. W., P. C. Gallacher, and P. Muller (1985a), Wind direction and equilibrium mixed layer depth: General theory, *J. Phys. Oceanogr.*, *15*, 1325–1331.

Garwood, R. W., P. Muller, and P. C. Gallacher (1985b), Wind direction and equilibrium mixed layer depth in the tropical Pacific Ocean, *J. Phys. Oceanogr.*, *15*, 1332–1338.

Gates, W. L. (2004), Derivation of the equations of atmospheric motions in oblate spherical coordinates, *J. Atmos. Sci.*, *61*, 2478–2487.

Gerkema, T. (2006), Internal-wave reflection from uniform slopes: Higher harmonics and Coriolis effects, *Nonlinear Processes Geophys.*, *13*, 265–273.

Gerkema, T., and V. I. Shrira (2005a), Near-inertial waves on the "nontraditional" β plane, *J. Geophys. Res.*, *110*, C01003, doi:10.1029/2004JC002519.

Gerkema, T., and V. I. Shrira (2005b), Near-inertial waves in the ocean: Beyond the 'traditional approximation,' *J. Fluid Mech.*, *529*, 195–219.

Gerkema, T., and V. I. Shrira (2006), Non-traditional reflection of internal waves from a sloping bottom, and the likelihood of critical reflection, *Geophys. Res. Lett.*, *33*, L06611, doi:10.1029/2005GL025627.

Gerkema, T., F. P. A. Lam, and L. R. M. Maas (2004), Internal tides in the Bay of Biscay: Conversion rates and seasonal effects, *Deep Sea Res., Part II*, *51*, 2995–3008.

Grimshaw, R. (1975a), Internal gravity waves: Critical layer absorption in a rotating fluid, *J. Fluid Mech.*, *70*, 287–304.

Grimshaw, R. H. J. (1975b), A note on the β-plane approximation, *Tellus*, *27*, 351–356.

Guillot, T. (2005), The interiors of giant planets: Models and outstanding questions, *Annu. Rev. Earth Planet. Sci.*, *33*, 493–530.

Haeusser, T. M., and S. Leibovich (1997), Amplitude and mean drift equations for the oceanic Ekman layer, *Phys. Rev. Lett.*, *79*(2), 329–332.

Haeusser, T. M., and S. Leibovich (2003), Pattern formation in the marginally unstable Ekman layer, *J. Fluid Mech.*, *479*, 125–144.

Harlander, U., and L. R. M. Maas (2006), Characteristics and energy rays of equatorially trapped, zonally symmetric internal waves, *Meteorol. Z.*, *15*(4), 439–450.

Heimpel, M., and J. Aurnou (2007), Turbulent convection in rapidly rotating spherical shells: A model for equatorial and high latitude jets on Jupiter and Saturn, *Icarus*, *187*, 540–557.

Heimpel, M., J. Aurnou, and J. Wicht (2005), Simulation of equatorial and high-latitude jets on Jupiter in a deep convection model, *Nature*, *438*, 193–196.

Hendershott, M. C. (1981), Long waves and ocean tides, in *Evolution of Physical Oceanography*, edited by B. A. Warren and C. Wunsch, pp. 292–341, MIT Press, Cambridge, Mass.

Hollerbach, R., and R. R. Kerswell (1995), Oscillatory internal shear layers in rotating and precessing flows, *J. Fluid Mech.*, *298*, 327–339.

Hua, B. L., D. W. Moore, and S. le Gentil (1997), Inertial nonlinear equilibration of equatorial flows, *J. Fluid Mech.*, *331*, 345–371.

Hughes, B. (1964), Effect of rotation on internal gravity waves, *Nature*, *201*, 798–801.

Huthnance, J. M. (1978), Inertial waves and an initial-value problem for a thin spherical rotating fluid shell, *J. Fluid Mech.*, *86*, 273–288.

Hylleraas, E. A. (1939), Über die Schwingungen eines stabil geschichteten, durch Meridiane begrenzten Meeres, *Astrophys. Nor.*, *III*(6), 139–164.

Ingersoll, A. P., and D. Pollard (1982), Motion in the interiors and atmospheres of Jupiter and Saturn—Scale analysis, anelastic equations, barotropic stability-criterion, *Icarus*, *52*, 62–80.

Ioannou, P. J., and R. S. Lindzen (1993a), Gravitational tides in the outer planets. I. Implications of classical tidal theory, *Astrophys. J.*, *406*, 252–265.

Ioannou, P. J., and R. S. Lindzen (1993b), Gravitational tides in the outer planets. II. Interior calculations and estimation of the tidal dissipation factor, *Astrophys. J.*, *406*, 266–278.

Israeli, M. (1972), On trapped oscillations of rotating fluids in spherical shells, *Stud. Appl. Math.*, *L1*, 219–237.

Joyce, T. M., R. Lukas, and E. Firing (1988), On the hydrostatic balance and equatorial geostrophy, *Deep Sea Res., Part A*, *35*, 1255–1257.

Kasahara, A. (2003a), The roles of the horizontal component of the Earth's angular velocity in nonhydrostatic linear models, *J. Atmos. Sci.*, *60*, 1085–1095.

Kasahara, A. (2003b), On the nonhydrostatic atmospheric models with inclusion of the horizontal component of the Earth's angular velocity, *J. Meteorol. Soc. Jpn.*, *81*(5), 935–950.

Kasahara, A. (2004), Reply, *J. Atmos. Sci*, *61*, 1987–1991.

Kasahara, A., and J. M. Gary (2006), Normal modes of an incompressible and stratified fluid model including the vertical and horizontal components of Coriolis force, *Tellus, Ser. A*, *58*, 368–384.

Kerswell, R. R. (1995), On the internal shear layers spawned by the critical regions in oscillatory Ekman boundary layers, *J. Fluid Mech.*, *298*, 311–325.

Laplace, P.-S. (1798), *Traité de mécanique céleste*, vol. 1, 368 pp., Crapelet, Paris.

Laplace, P.-S. (1878), *Oeuvres complètes de Laplace*, vol. 1, 395 pp., Gauthier-Villars, Paris.

Lavrovskii, E. K., I. P. Semenova, L. N. Slezkin, and V. V. Fominykh (2000), Mediterranean lenses as liquid gyroscopes in the ocean, *Dokl. Phys.*, *45*(11), 606–609.

LeBlond, P. H., and L. A. Mysak (1978), *Waves in the Ocean*, 602 pp., Elsevier, Amsterdam.

Leibovich, S., and S. K. Lele (1985), The influence of the horizontal component of Earth's angular velocity on the instability of the Ekman layer, *J. Fluid Mech.*, *150*, 41–87.

Longuet-Higgins, M. S. (1964), Planetary waves on a rotating sphere, *Proc. R. Soc. London, Ser. A*, *279*, 446–473.

Lukas, R., and E. Lindstrom (1991), The mixed layer of the western equatorial Pacific Ocean, *J. Geophys. Res.*, *96*, 3343–3357.

Luyten, J. R., and J. C. Swallow (1976), Equatorial undercurrents, *Deep Sea Res. Oceanogr. Abstr.*, *23*, 999–1001.

Maas, L. R. M. (2001), Wave focusing and ensuing mean flow due to symmetry breaking in rotating fluids, *J. Fluid Mech.*, *437*, 13–28.

Maas, L. R. M. (2005), Wave attractors: Linear yet nonlinear, *Int. J. Bifurcation Chaos*, *15*(9), 2757–2782.

Maas, L. R. M., and U. Harlander (2007), Equatorial wave attractors and inertial oscillations, *J. Fluid Mech.*, *570*, 47–67.

Maas, L. R. M., and F. P. A. Lam (1995), Geometric focusing of internal waves, *J. Fluid Mech.*, *300*, 1–41.

Maniopoulou, A., and N. Andersson (2004), The traditional approximation in general relativity, *Mon. Not. R. Astron. Soc.*, *351*, 1349–1358.

Marshall, J., and F. Schott (1999), Open-ocean convection: Observations, theory, and models, *Rev. Geophys.*, *37*, 1–64.

Marshall, J., C. Hill, L. Perelman, and A. Adcroft (1997), Hydrostatic, quasi-hydrostatic, and nonhydrostatic ocean modeling, *J. Geophys. Res.*, *102*(C3), 5733–5752.

McWilliams, J. C., and E. Huckle (2006), Ekman layer rectification, *J. Phys. Oceanogr.*, *36*, 1646–1659.

Miles, J. W. (1974), On Laplace's tidal equations, *J. Fluid Mech.*, *66*, 241–260.

Miropol'sky, Y. Z. (2001), *Dynamics of Internal Gravity Waves in the Ocean*, 406 pp., Kluwer, Dordrecht.

Müller, D. (1992), Angular momentum budget of shallow waters on a rotating sphere, *Phys. Rev. A*, *45*, 5545–5555.

Müller, R. (1989), A note on the relation between the "traditional approximation" and the metric of the primitive equations, *Tellus, Ser. A*, *41*, 175–178.

Needler, G. T., and P. H. LeBlond (1973), On the influence of the horizontal component of the Earth's rotation on long period waves, *Geophys. Fluid Dyn.*, *5*, 23–46.

Ogilvie, G. I., and D. N. C. Lin (2004), Tidal dissipation in rotating giant planets, *Astrophys. J.*, *610*, 477–509.

Phillips, N. A. (1966), The equations of motion for a shallow rotating atmosphere and the "traditional approximation," *J. Atmos. Sci.*, *23*, 626–628.

Phillips, N. A. (1968), Reply, *J. Atmos. Sci*, *25*, 1155–1157.

Phillips, N. A. (1970), Reply, *J. Atmos. Sci*, *27*, 506.

Phillips, O. M. (1966), *The Dynamics of the Upper Ocean*, 261 pp., Cambridge Univ. Press, Cambridge, UK.

Pickart, R. S., D. J. Torres, and R. A. Clarke (2002), Hydrography of the Labrador Sea during active convection, *J. Phys. Oceanogr.*, *32*, 428–457.

Pingree, R. D., and A. L. New (1991), Abyssal penetration and bottom reflection of internal tidal energy into the Bay of Biscay, *J. Phys. Oceanogr.*, *21*, 28–39.

Price, J. F., and M. A. Sundermeyer (1999), Stratified Ekman layers, *J. Geophys. Res.*, *104*(C9), 20,467–20,494.

Proudman, J. (1948), The applicability of Laplace's differential equations of the tides, *Int. Hydrogr. Rev.*, *25*(2), 122–129.

Raymond, W. H. (2000), Equatorial meridional flows: Rotationally induced circulations, *Pure Appl. Geophys.*, *157*, 1767–1779.

Raymond, W. H. (2001), Kelvin waves: Rotationally induced circulations, *Dyn. Atmos. Oceans*, *34*, 23–43.

Rhines, P. B. (1975), Waves and turbulence on a beta-plane, *J. Fluid Mech.*, *69*, 417–443.

Richards, K., and H. Banks (2002), Characteristics of interleaving in the western equatorial Pacific, *J. Geophys. Res.*, *107*(C12), 3231, doi:10.1029/2001JC000971.

Richardson, P. L., and D. M. Fratantoni (1999), Float trajectories in the deep western boundary current and deep equatorial jets of the tropical Atlantic, *Deep Sea Res., Part II*, *46*, 305–333.

Riemenschneider, U., and V. A. Sheremet (2006), Ball release experiments on a centrifuge: Misalignment between the buoyancy force and the axis of rotation, *J. Fluid Mech.*, *564*, 435–454.

Rieutord, M., and L. Valdettaro (1997), Inertial waves in a rotating spherical shell, *J. Fluid Mech.*, *341*, 77–99.

Rieutord, M., B. Georgeot, and L. Valdettaro (2001), Inertial waves in a rotating spherical shell: Attractors and asymptotic spectrum, *J. Fluid Mech.*, *435*, 103–144.

Saint-Guily, B. (1970), On internal waves. Effects of the horizontal component of the Earth's rotation and of a uniform current, *Dtsch. Hydrogr. Z.*, *23*(1), 16–23.

Savonije, G. J., and J. C. B. Papaloizou (1997), Non-adiabatic tidal forcing of a massive, uniformly rotating star—II. The low-frequency, inertial regime, *Mon. Not. R. Astron. Soc.*, *291*, 633–650.

Savonije, G. J., J. C. B. Papaloizou, and F. Alberts (1995), Non-adiabatic tidal forcing of a massive, uniformly rotating star, *Mon. Not. R. Astron. Soc.*, *277*, 471–496.

Schopp, R., and A. Colin de Verdière (1997), Taylor columns between concentric spheres, *Geophys. Astrophys. Fluid Dyn.*, *86*, 43–73.

Semenova, I. P., and L. N. Slezkin (2003), Dynamically equilibrium shape of intrusive vortex formations in the ocean, *Fluid Dyn.*, *38*(5), 663–669.

Send, U., C. Eden, and F. Schott (2002), Atlantic equatorial deep jets: Space-time structure and cross-equatorial fluxes, *J. Phys. Oceanogr.*, *32*, 891–902.

Sheremet, V. A. (2004), Laboratory experiments with tilted convective plumes on a centrifuge: A finite angle between the buoyancy force and the axis of rotation, *J. Fluid Mech.*, *506*, 217–244.

Solberg, H. (1928), Integrationen der atmosphärischen Störungs-gleichungen. Erster Teil: Wellenbewegungen in rotierenden, in-kompressiblen Flüssigkeitsschichten, *Geofys. Publ.*, *V*(9), 1–120.

Solberg, H. (1936), Über die freien Schwingungen einer homoge-nen Flüssigkeitsschicht auf der rotierenden Erde I, *Astrophys. Nor.*, *I*(7), 237–340.

Stern, M. E. (1963), Trapping of low frequency oscillations in an equatorial 'boundary layer,' *Tellus*, *15*, 246–250.

Stewartson, K. (1971), On trapped oscillations of a rotating fluid in a thin spherical shell, *Tellus*, *23*, 506–510.

Stewartson, K. (1972a), On trapped oscillations of a rotating fluid in a thin spherical shell II, *Tellus*, *24*, 283–287.

Stewartson, K. (1972b), On trapped oscillations in a slightly vis-cous rotating fluid, *J. Fluid Mech.*, *54*, 749–761.

Stewartson, K., and J. A. Rickard (1969), Pathological oscillations of a rotating fluid, *J. Fluid Mech.*, *5*, 577–592.

Straneo, F., M. Kawase, and S. C. Riser (2002), Idealized models of slantwise convection in a baroclinic flow, *J. Phys. Oceanogr.*, *32*, 558–572.

Taylor, G. I. (1923), Experiments on the motion of solid bodies in rotating fluids, *Proc. R. Soc. London, Ser. A*, *104*, 213–218.

Thuburn, J., N. Wood, and A. Staniforth (2002a), Normal modes of deep atmospheres. I: Spherical geometry, *Q. J. R. Meteorol. Soc.*, *128*, 1771–1792.

Thuburn, J., N. Wood, and A. Staniforth (2002b), Normal modes of deep atmospheres. II: *f*-*F*-plane geometry, *Q. J. R. Meteorol. Soc.*, *128*, 1793–1806.

Tolstoy, I. (1963), The theory of waves in stratified fluids including the effects of gravity and rotation, *Rev. Mod. Phys.*, *35*(1), 207–230.

Tritton, D. J. (1978), Turbulence in rotating fluids, in *Rotating Fluids in Geophysics*, edited by P. H. Roberts and A. M. Soward, pp. 105–138, Academic, London.

van Aken, H. M., L. R. M. Maas, and H. van Haren (2005), Ob-servations of inertial wave events near the continental slope off Goban Spur, *J. Phys. Oceanogr.*, *35*, 1329–1340.

van der Toorn, R., and J. T. F. Zimmerman (2008), On the spherical approximation of the geopotential in Geophysical Fluid Dy-namics and the use of a spherical coordinate system, *Geophys. Astrophys. Fluid Dyn*, in press.

van Haren, H. (2005), Sharp near-equatorial transitions in inertial motions and deep-ocean step-formation, *Geophys. Res. Lett.*, *32*, L01605, doi:10.1029/2004GL021630.

van Haren, H. (2006), Asymmetric vertical internal wave pro-pagation, *Geophys. Res. Lett.*, *33*, L06618, doi:10.1029/2005GL025499.

van Haren, H., and C. Millot (2004), Rectilinear and circular in-ertial motions in the western Mediterranean Sea, *Deep Sea Res., Part I*, *51*, 1441–1455.

van Haren, H., and C. Millot (2005), Gyroscopic waves in the Mediterranean Sea, *Geophys. Res. Lett.*, *32*, L24614, doi:10.1029/2005GL023915.

van Haren, H., L. R. M. Maas, and H. van Aken (2002), On the nature of internal wave spectra near a continental slope, *Geophys. Res. Lett.*, *29*(12), 1615, doi:10.1029/2001GL014341.

Vasavada, A. R., and A. P. Showman (2005), Jovian atmospheric dynamics: An update after Galileo and Cassini, *Rep. Prog. Phys.*, *68*, 1935–1996.

Verkley, W. T. M. (1990), On the beta plane approximation, *J. Atmos. Sci.*, *47*, 2453–2460.

Veronis, G. (1959), Cellular convection with finite amplitude in a rotating fluid, *J. Fluid Mech.*, *5*, 401–435.

Veronis, G. (1963a), On the approximations involved in transform-ing the equations of motion from a spherical surface to the β-plane. I. Barotropic systems, *J. Mar. Res.*, *21*, 110–124.

Veronis, G. (1963b), On the approximations involved in transform-ing the equations of motion from a spherical surface to the β-plane. II. Baroclinic systems, *J. Mar. Res.*, *21*(3), 199–204.

Veronis, G. (1968), Comments on Phillips' proposed simplification of the equations of motion for a shallow rotating atmosphere, *J. Atmos. Sci.*, *25*, 1154–1155.

Walter, M., C. Mertens, and M. Rhein (2005), Mixing estimates from a large-scale hydrographic survey in the North Atlantic, *Geophys. Res. Lett.*, *32*, L13605, doi:10.1029/2005GL022471.

Walton, I. C. (1975), On waves in a thin rotating spherical shell of slightly viscous fluid, *Mathematika*, *22*, 46–59.

Wangsness, R. K. (1970), Comments on "The equations of motion for a shallow rotating atmosphere and the 'traditional approxima-tion' ," *J. Atmos. Sci.*, *27*, 504–506.

White, A. A., and R. A. Bromley (1995), Dynamically consistent, quasi-hydrostatic equations for global models with a complete representation of the Coriolis force, *Q. J. R. Meteorol. Soc.*, *121*, 399–418.

White, A. A., B. J. Hoskins, I. Roulstone, and A. Staniforth (2005), Consistent approximate models of the global atmosphere: Shal-low, deep, hydrostatic, quasi-hydrostatic and non-hydrostatic, *Q. J. R. Meteorol. Soc.*, *131*, 2081–2107.

Wippermann, F. (1969), The orientation of vortices due to instabil-ity of the Ekman-boundary layer, *Beitr. Phys. Atmos.*, *42*, 225–244.

Wirth, A., and B. Barnier (2006), Tilted convective plumes in numerical experiments, *Ocean Modell.*, *12*, 101–111.

Wirth, A., and B. Barnier (2008), Mean circulation and structures of tilted ocean deep convection, *J. Phys. Oceanogr.*, *38*, 803–816.

Yano, J., O. Talagrand, and P. Drossart (2005), Deep two-dimen-sional turbulence: An idealized model for atmospheric jets of the giant outer planets, *Geophys. Astrophys. Fluid Dyn.*, *99*, 137–150.

Zikanov, O., D. N. Slinn, and M. R. Dhanak (2003), Large-eddy simulations of the wind-induced turbulent Ekman layer, *J. Fluid Mech.*, *495*, 343–368.

————————————————
T. Gerkema, L. R. M. Maas, H. van Haren, and J. T. F. Zimmerman, Royal Netherlands Institute for Sea Research, P.O. Box 59, NL-1790 AB Den Burg, Texel, Netherlands. (gerk@nioz.nl)